Policy Research Working Paper 10240

Wave Reduction by Mangroves during Cyclones in Bangladesh

Implementing Nature-Based Solutions for Coastal Resilience

Alejandra Gijón Mancheño
Vincent Vuik
Bregje K. van Wesenbeeck
S.N. (Bas) Jonkman
Roelof Moll
Swarna Kazi
Ignacio Urrutia
Mathijs van Ledden

WORLD BANK GROUP
Urban, Disaster Risk Management, Resilience and Land Global Practice
November 2022

Policy Research Working Paper 10240

Abstract

This paper investigates how mangrove foreshores can be integrated into embankment designs in Bangladesh. The effect of mangroves on surges has already been studied for the design conditions of Bangladesh. However, the impact of wave attenuation by mangroves on embankment designs is not known. A model is thus developed to estimate the wave height reduction by a mangrove forest, and how such wave attenuation would influence the design of a landward embankment. Model simulations suggest that mangrove belts with a width between 100 and 1,000 meters (perpendicular to the coast) could provide wave attenuation rates between 7 and 55 percent (compared to a situation without mangroves) at potential afforestation sites identified in previous studies. Such wave attenuation rates would reduce the embankment height by 0.09–0.30 meters, diminish the slope revetment thickness by 13–46 percent, and decrease the wave shear stresses at the embankment toe up to 25–70 percent. Relatively wider mangrove belts not only cause a larger reduction of the embankment design requirements, but also host larger biodiversity and are more resilient against pests and extreme events. The model results are highly sensitive to the mangrove properties, and collecting data on the local mangrove species is recommended to reduce uncertainty in the predictions. Moreover, the results also suggest that trees older than 10–20 years might collapse during storms. Expanding the mangrove stability model, including other pioneer species in the analysis, and exploring the option of canopy pruning are thus advised to ensure the integrity of any future afforestation efforts. Overall, this paper provides a methodology that could be applied to design nature-based solutions in Bangladesh.

This paper is a product of the Urban, Disaster Risk Management, Resilience and Land Global Practice. This research received financial support from the European Union (EU) in the framework of the EU-SAR Capacity Building for Disaster Risk Management Program, managed by the Global Facility for Disaster Reduction and Recovery (GFDRR). It is part of a larger effort by the World Bank to provide open access to its research and make a contribution to development policy discussions around the world. Policy Research Working Papers are also posted on the Web at http://www.worldbank.org/prwp. The authors may be contacted at a.gijonmancheno-1@tudelft.nl, mvanledden@worldbank.org, and skazi1@worldbank.org.

Wave Reduction by Mangroves during Cyclones in Bangladesh

Implementing Nature-Based Solutions for Coastal Resilience

Alejandra Gijón Mancheño[1], Vincent Vuik[1,2], Bregje K. van Wesenbeeck[1,3], S.N. (Bas) Jonkman[1], Roelof Moll[1], Swarna Kazi[4], Ignacio Urrutia[4], Mathijs van Ledden[4]

[1]Delft University of Technology

[2]Royal Haskoning

[3]Deltares

[4]World Bank

Keywords: building with nature, mangroves, wave attenuation, flood risk reduction, hybrid flood protection, embankments, climate change, resilience, Bangladesh.

JEL Classification: Q54, Q56, Q57.

1. Introduction

Bangladesh is one of the most vulnerable countries to coastal flooding due to its exposure to frequent cyclones, massive rainfall events, and due to its large population density in low-lying areas (Khan, 1992; Jakobsen et al., 2005; Eckstein et al, 2018). To mitigate flood hazards, the coastal system of Bangladesh is defended by a system of 6,000 km of peripherical embankments that enclose 139 polders (Figure 1.1). The construction of the embankment system in the 1960s-1970s had a positive impact on the economy of the country, as it increased agricultural productivity by 200%-300% at some polders (Nishat, 1988). However, the original structures were not designed to withstand coastal surges (Islam, 2011), and lack of maintenance over time resulted in tidal intrusion, increasing flood risk, and lower agricultural productivity (Naz and Buisson, 2015; Awal and Islam, 2020).

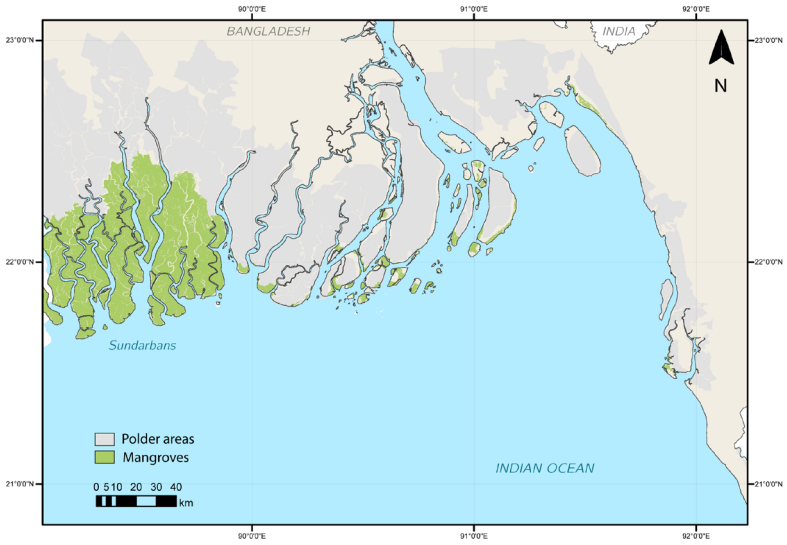

Figure 1.1. Coastal system of Bangladesh, from Gijón Mancheño et al. (2021). Bangladesh is home of 60% of the Sundarbans, the largest mangrove forest in the world. The mangrove areas in Bangladesh are shown in green for the situation of 2018 (Global Forest Watch, 2020). The coastal area of Bangladesh is protected by a system of 6000 km of embankments that form 139 polders (in grey).

To increase the resilience of the coastal system, the Coastal Embankment Improvement Project Phase 1 (CEIP-1) focused on upgrading the safety of 10 polders to a 25-year level of protection. The CEIP project covered several activities to increase safety against flood

hazards, such as structure reinforcement and afforestation at the seaward side of the embankments (World Bank, 2013). Afforestation plans included both planting of commercial species for economic purposes and mangrove planting for coastal protection. Bangladesh has large mangrove afforestation potential, as it is the home of 60% of the Sundarbans, the largest mangrove forest in the world, and it has considerable experience in mangrove afforestation, with 150,000 ha of planted mangroves since the 1960s (Saenger and Siddiqi, 1993). The modeling work of Dasgupta et al. (2017) showed that mangrove afforestation in Bangladesh would likely have a small effect on surge heights. Nevertheless, mangroves could significantly reduce the flow velocities and erosion near embankments (Dasgupta et al., 2017). Mangrove belts could also provide additional protection to coastal structures by attenuating short waves, and thus reducing the wave loads acting on them and the wave runup. Potential locations for mangrove afforestation seaward from embankments have been identified for Bangladesh (Gijón Mancheño et al., 2021), however, their effect on the wave loads acting on the structures and on wave runup has not been evaluated.

This paper quantifies the potential wave height reduction by a mangrove belt planted on the seaside of embankments, and how such wave attenuation would impact embankment designs. Wave energy attenuation by mangroves is calculated by integrating the energy dissipation caused by the trees, and by solving the wave energy balance as done by Mendez and Losada (2004). The wave model is applied using the hydraulic properties of *Sonneratia apetala*, which is a mangrove pioneer species in Bangladesh, obtained from the analysis of field pictures and from a literature study. The potential failure of the trees by either overturning or trunk breakage is estimated for the design conditions using empirical expressions developed in agroforestry studies. Finally, the calculated wave heights are used as an input in the design formulas of embankments to evaluate how the presence of a mangrove belt would affect their height, slope protection needs, and the shear stresses at their toe.

2. Theoretical background

2.1. Coastal protection by mangroves

Mangroves reduce coastal erosion and flooding through several mechanisms. During storms, strong winds push the sea water towards the coast, causing an increase of water level

denoted as surge. Mangroves have a limited effect on the surge heights (Figure 2.1), with observed attenuation rates up to 24 cm per km of forest (Krauss et al., 2009; Dasgupta et al, 2017; Montgomery et al., 2018), as surge generation is a process that occurs over length scales of hundreds of kilometers. This implies that forest lengths of at least 12-20 km would be needed to fully attenuate surge heights of 3-5 m. In addition, surge reduction by mangroves is very much dependent on spatial configuration of the forest and creek structure within the forest, with channelized areas having an even lower effect on surge heights (Montgomery et al., 2018).

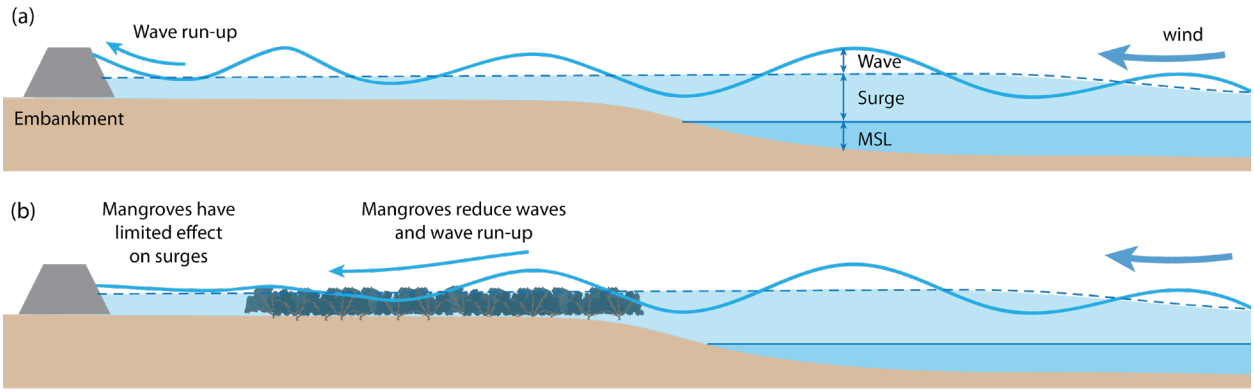

Figure 2.1. (a) Design water levels at a profile without mangroves. Wind forcing during extreme events pushes the sea towards the land, increasing the water level with respect to mean sea level (MSL), an effect denoted as surge. Storm winds also generate waves that propagate towards the coast, and runup on coastal structures after breaking. (b) Mangrove belts with lengths below 1 km have small effect on surges, as surges occur on much larger length scales. However, mangroves can significantly attenuate wind waves, their induced runup, and thus reduce the design water levels of coastal embankments. Wave reduction by mangroves also decreases the required slope protection and erosion at the embankments. The interaction between wave radiation stresses and aquatic vegetation can also induce an additional set-up (van Rooijen et al., 2018), however, this effect has not been quantified for mangroves.

Storm winds also generate swell and wind waves, which can be largely reduced by the dense branch and root systems of mangroves (Mazda et al., 1997; Massel et al., 1999; Bao, 2011; Horstman et al., 2014). Reported rates of wave attenuation over 100 m of forest vary between 5%-100% (see Table 1), with increasing attenuation for shorter waves and denser forests. Extrapolating such attenuation rates to other mangrove sites is not straightforward, as most studies report the full wave reduction through a transect including the effect of wave breaking, bottom friction, and wave energy dissipation by the vegetation, and do not separate the effect of mangroves from the other hydrodynamic processes. Moreover, existing field

measurements were collected during calm conditions in which the water depth through the forest was very shallow. Larger water levels and relatively longer waves during storms could cause relatively less wave height reduction compared to situations of calmer weather.

Table 1. Wave attenuation rates by mangroves from the literature, expanded from Horstman et al. (2014). The reported wave attenuation rates represent the total wave height reduction with respect to the incoming wave height, including wave breaking and bottom friction. For each study, the incoming wave height (m) and period (s), the dominant vegetation species, and the mean tree height (m) and tree density (trees per m^2), are reported.

Author	W. Attenuation per m (%)	Wave height (m)	Wave period (s)	Species	Height (m)	Density (tr/m2)
Mazda et al. (1997)	0,01-0,10	-	5-8	Kandelia candel	0,2	1
Mazda et al. (1997)	0,08-0,15	-	5-8	Kandelia candel	0,45	0,85
Mazda et al. (1997)	0,15-0,22	-	5-8	Kandelia candel	1,1	0,88
Mazda et al. (2006)	0,20-0,60	0,11-0,16	8-10	Sonneratia sp.	-	0,08
Quartel et al. (2007)	0,40-1,20	0,15-0,25	4-6	Kandelia candel	2,5	-
Bao (2011)	0,55-1,00	0,15-0,27	-	Mixed	1-11	0,2-1,3
Brinkman (2006)	0,28-0,50	0,01-0,07	2	Mixed	-	-
Brinkman (2006)	0,38-1,88	0,08-0,15	2	Bruguiera sp.	-	-
Brinkman (2006)	2,25-2,50	0,04-0,25	6	Mixed	-	-
Horstman et al. (2014)	0,14-1,20	0,01-0,20	2,5-5	Mixed	-	-
Sanchez-Nuñez et al. (2020)	0,15-0,45	0,00-0,20	-	Rhizophora mangle	-	-
Bëst et al. (2022)	0,20-0,32	0,00-0,70	4-5	Mixed	0,07-13	0-0,7

Wave attenuation seaward from a dike can reduce the wave-induced runup, decreasing the required height and slope protection needs of coastal structures (Vuik et al, 2016, 2018 & 2019). Moreover, mangroves can increase the resilience of embankments against erosion and sea level rise. Modeling studies suggest that reduction of current velocities by mangroves can reach 91% for a mangrove forest length of 100 m (Dasgupta et al., 2017). Current and wave attenuation by mangroves decreases erosion at the coast and favors sediment accumulation inside the forest (Trampanya et al., 2006). Sediment deposition at coastal areas in turn increases the bed level, which can partly or totally counteract rising sea levels (Lovelock et al., 2015; Sasmito et al., 2016; Woodroffe et al., 2016.; McKee et al., 2018). For instance, analysis of geological records suggest that mangroves were able to vertically keep up with up to 6-7 mm of sea level rise per year by inducing sediment accretion and by biomass accumulation (Saintilan et al., 2020). Higher bed levels reduce the wave loads on the dikes

even further, as they decrease the maximum waves that can propagate towards the embankment without breaking.

Although the previous functions result in sheltering of the coast from extreme events, applying mangroves to reduce the wave loads on dikes requires considering several limiting factors. Firstly, mangroves have specific habitat requirements, and they may not grow at every location. Mangroves grow at intertidal areas with low wave action, and sufficient freshwater and sediment input (Alongi, 2002), and different mangrove species have specific requirements in terms of temperature, inundation, and salinity levels that they can tolerate. Potential sites for mangrove establishment have been mapped in Bangladesh (Gijón Mancheño et al., 2021), indicating locations where mangroves could grow naturally, and those where erosion mitigation would be necessary for mangrove colonization. However, the potential wave load reduction by mangroves at such sites has not been investigated, which hinders accounting for the effect of mangroves on embankment designs in future CEIP programs.

2.2. Mangrove geometry

Wave reduction by mangroves is highly dependent on the location of the trees on the tidal profile and on their geometry. Mangrove species often grow in distinct bands between mean sea level (MSL) and mean high water (MHW), depending on their relative tolerance to inundation (Snedaker, 1982). Some species, denoted as pioneers, have a relatively higher tolerance to salinity and are the first to colonize at locations near MSL. Within the salt-tolerant species found in Bangladesh, *Sonneratia apetala* (locally known as Keora) and *Avicennia officinalis* (locally known as Baen) are the pioneers with highest planting survival (Saenger and Siddiqi, 1993). Since *S. apetala* is the most planted species, for which there is also most available information about its geometrical and structural properties, this species is chosen for further analysis.

At sites where mangroves were not present before, such as on newly accreted land, mangrove trees will need time to colonize and grow. Ecologic studies suggest that mangroves can reach their full height in 10 years (Wang et al., 2021), and their wave attenuation capacity will increase as the surface area of the tree enlarges by growth of the trunk diameter, and by increasing the size and number of branches (Maza et al., 2021).

However, mangrove growth is highly site-specific, as mangrove development is dependent on several biophysical conditions, such as local temperatures (Simard et al., 2019), salinity (Rahman et al., 2020), and soil chemistry among other parameters. Existing data of *S. apetala* growth is shown in Figure 2.2 for planted *S. apetala* trees in China (Wang et al., 2021), and for planted and natural trees in Bangladesh (Islam et al., 2016; Uddin and Hossain, 2013). Planted trees have comparable trunk diameters and heights in China and Bangladesh until they are 20 years old (Figure 2.2, b-c). Beyond that age, the height of Chinese specimens stabilizes remains between 5-12 m, whereas Bangladeshi trees of the same age reach larger heights, between 16-18 m (Figure 2.2 c). This is consistent with *S. apetala* being a native species in the Sundarbans, which was introduced for afforestation in China in the 1980s (Xin et al., 2013), but a wider dataset would be needed to generalize the previous observations. Field measurements in the Sundarbans show that *S. apetala* trees reach mean heights of 17.97 m (± 5.9 m) and mean trunk diameters at breast height of 29.35 cm (± 12.84 cm) (Rahman et al., 2021).

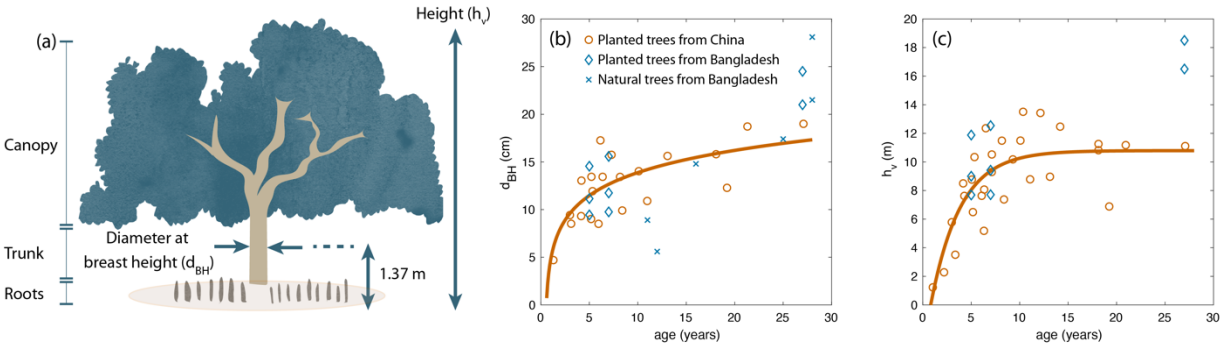

Figure 2.2. (a) Structure of a Sonneratia apetala tree, consisting of pneumatophore root mat, trunk, and canopy (branches and leaves). (b-c) Changes in S. apetala properties over time for plantations in China (Wang et al., 2021) and Bangladesh (Islam et al., 2016; Uddin et al., 2013), and for natural trees at the north of the Sundarbans (Rahman et al., 2020), where (b) shows the diameter at breast height (d_{BH}) in cm, and (c) the tree height (h_v) in m. The orange fit lines are from Wang et al. (2021).

The structure of *S. apetala* trees consists of: (1) pneumatophore roots, (2) trunk, (3) a canopy formed by branches and leaves (Figure 2.2, a). Pneumatophores are vertical roots that rise from the buried root structure and emerge through the ground. These vertical roots function as snorkels that supply oxygen to the tree. Pneumatophore height also varies as trees grow (Table 2) from 0.08 m for 2-year-old specimens (Chen et al., 2021), up to 1.04 m for very mature trees (Dasgupta et al., 2017).

Table 2. Properties of the pneumatophores of S. apetala trees from the literature. Each row indicates the authors of the study, the country where the measurements were taken, and the vegetation properties: root height (m), root diameter (m) root density (roots per m^2), trunk diameter at breast height (d_{BH}, in m), tree height (m), tree density (trees per m^2), and age (years).

Study	Country	Root height	Root diameter	Root density	d_{BH}	Height	Density	Age
		[m]	*[m]*	*[roots/m2]*	*[m]*	*[m]*	*[trees/m2]*	*[year]*
Chen et al. (2021)	China	0.08	-	-	0.07	2.27	0.01	2.08
Mazda et al. (2005)	Vietnam	0.14	0.007	131	0.12	-		-
Duan et al (2021)	China	0.18	0.008	-	0.35	14.8	0.17	-
Zhang et al. (2019)	China	0.12	-	253	-	18.3	0.17	-
Dasgupta et al. (2017)	Bangladesh	1.04	0.15	-	0.51	-	0.01-0.04	-

Although the data in Figure 2.2 provides an indication of how the trunk diameter and tree height change as *S. apetala* trees grow, the evolution of the total frontal tree with age is not known. In the existing literature the equivalent width for mangrove canopies is defined using 3 approaches, as shown in Figure 2.3.

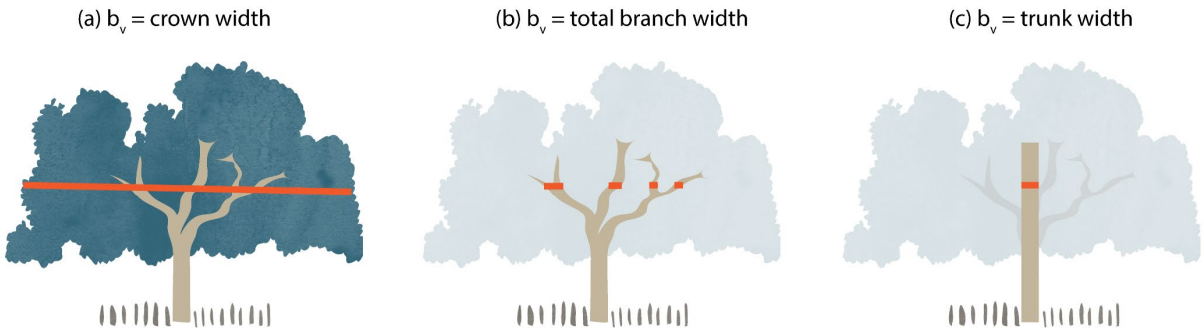

Figure 2.3. Approaches to define the canopy width of a tree for wave modeling. (a) Assuming the total crown width is representative of the tree width, (b) assuming an equivalent width representative of the total branch area per unit height, (c) assuming the trunk width as representative of the tree width.

Some authors, such as Zhang et al. (2021), assume that the width of the canopy is given by the outer contour of the tree crown (Figure 2.3, a). This approach considers the canopy to be fully solid and neglects the voids and empty areas between branches and leaves. Other authors such as Mazda et al. (1997) or Quartel et al. (2007) remove the voids and use the total branch and leaf area to estimate the resistive area of the tree. However, leaves were found to have a small effect on wave attenuation in flume experiments with willow trees (van Wesenbeeck et al., 2022), as leaves will streamline during extreme events, or may be pulled

over by wind and/or waves (van Hespen et al., 2021). Including the full leaf area in b_v predictions most likely overpredicts the effect of trees during extreme events.

Conversely, some authors completely neglect the effect of canopy leaves and branches and assume that the tree area above the root system is given by the area of the trunk (Massel et al., 1999), as shown in Figure 2.3 (c). This assumption may hold for measurements taken during calm conditions, where the water levels remain below the canopy, and/or for very tall trees for which the canopy is never submerged. However, canopies may be the largest contributor to wave attenuation for relatively higher water levels (van Wesenbeeck et al., 2022) and for shorter trees. Under such conditions, using the trunk width as the equivalent width b_v would likely underestimate the tree area, and the wave dissipation by a tree.

The effective canopy width for wave attenuation purposes is likely to correspond with an intermediate situation (Figure 2.3, b). For willow trees, tree trunk and branch models were developed and successfully used to predict wave attenuation by Kalloe et al. (2022). However, the vertical distribution of the canopy branch area has not been quantified for mangroves.

2.3. Mangrove stability against storms

Although mangroves can protect the coast from storm events, they can also be degraded by the impact of winds and waves. Hurricanes and cyclones can directly damage mangroves by defoliating them, by breaking their trunk or branches, or by overturning them (Figure 2.4). Extreme events can also damage mangroves by altering their habitat, for instance, by changing the local hydrology, topography, sediment conditions, or the forest structure (Herrera-Silveira et al., 2022). In Bangladesh the cyclone Sidr (2007) damaged between 11% (Carrol et al., 2019) and 45% (Bhowmik and Cabral, 2011) of the total area of the Sundarbans. Even though mangrove vegetation can recover over time (Carrol et al., 2019), its degradation implies that the hinterland is less sheltered by the vegetation (Pendleton et al., 2012). Several studies have investigated the potential effect of restored mangrove foreshores on flood risk (Menéndez et al., 2020; van Zelst et al., 2021), but they often assume the vegetation fully grown and/or neglect vegetation failure.

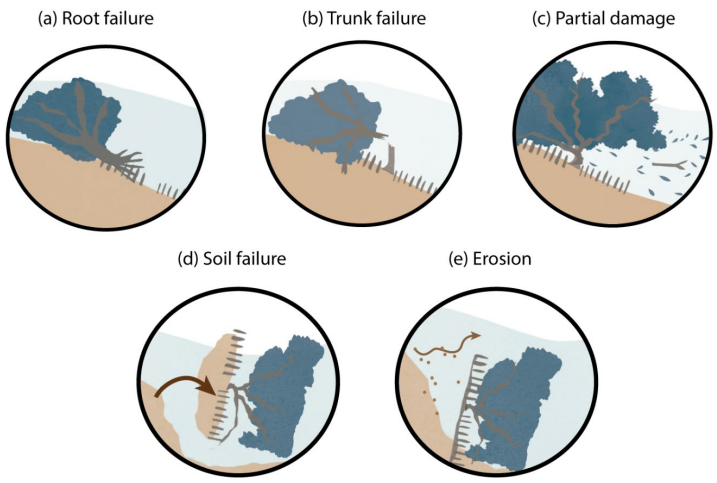

Figure 2.4. Potential mechanical failure modes of mangrove trees, such as (a) root failure leading to tree overturning, (b) trunk breakage, (c) damage due to loss of branches and leaves, (d) soil failure, and (e) erosion leading to profile scouring and tree overturning.

Although the extent of mangrove degradation has been quantified for different extreme events, mechanistic models for mangrove failure are lacking. Nevertheless, the failure mechanisms of tree breakage and overturning have been extensively studied for terrestrial trees exposed to wind forces (Gardiner et al., 2016). Models for wind loads and for the resistance of terrestrial trees against failure are presented in Appendix B.

Wave loads are not relevant for terrestrial trees, but they may also contribute to mangrove failure. The relative influence of wind and waves likely varies with the water level and vegetation height. For low water levels compared to the tree height, mangrove trees may fail due to wind action, whereas as trees are increasingly submerged, wave loads may have an increasing contribution on the total force acting on the trees. The lower density of the air compared to water also implies that lower flow velocities (compared to the wind speed) are needed to reach comparable forces (see Appendix B). However, considering that surge heights in Bangladesh often reach 3-5 m (Karim and Mimura, 2008; Zaman and Mondal, 2020), and that grown *S. apetala* trees can reach heights of 24 m, a significant part of the exposed tree area will be at the canopy. Mature trees will most likely be vulnerable to wind loads, whereas wave loads will be most important during the first years after mangrove establishment.

3. Methodology

This section describes the potential mangrove sites (Section 3.1), the method developed to quantify the effect of mangroves on embankment designs (Section 3.2), and the modeling scenarios (Section 3.3).

3.1. Potential mangrove sites in Bangladesh

The coastal system of Bangladesh is located on the north of the Bay of Bengal, on the Ganges-Brahmaputra-Meghna (GBM) delta. The western side of the coastal area is covered by 60% of the Sundarbans, the largest continuous mangrove forest in the world (Figure 1.1). The central part of the system consists of low-lying polder areas, whereas the east coast of the country is formed by smaller polders located on steeper ground. The climate of Bangladesh is characterized by several seasons: the hot pre-monsoon between March and May, the rainy monsoon between June and August, the post-monsoon between October-November, and the cool and dry winter between November and February. Cyclones occur yearly in Bangladesh, and severe cyclones with wind speeds varying between 90-119 km/hour hit the coastline on average every 3 years (Dasgupta et al., 2017). Surge heights often reach 3-5 m (Karim and Mimura, 2008; Zaman and Mondal, 2020), and observations suggest that 10 m water levels (consisting of surge plus tides) occur with a frequency of once in every 20 years (Dasgupta et al., 2014).

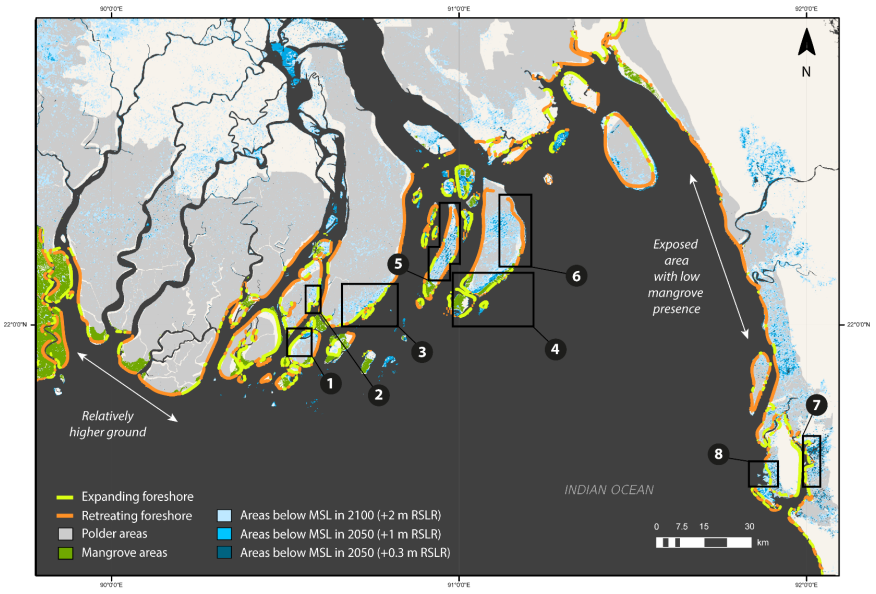

Figure 3.1. Potential sites for mangrove afforestation seaward from embankments from Gijón Mancheño et al. (2021)

Several potential sites for mangrove afforestation seaward from dikes have been identified in the coastal system of Bangladesh (Gijón Mancheño et al., 2021), which are shown in Figure 3.1. These afforestation sites were selected considering several criteria:

- Distance from existing mangroves, with locations within 10 km of a forest being considered favorable for colonization.
- Coastline behavior, with expanding coastlines (moving seaward) being suitable for natural colonization or planting, and eroding coastlines (moving landwards) requiring erosion-mitigation measures.
- Sites facing polders with low ground elevation are prioritized, as they could experience larger inundation depths in case of breaching of the embankments.

Out of the 8 potential sites shown in Figure 3.1, this study focuses on sites 1-6, as they would not require any erosion mitigation measures. The design conditions and associated embankment height for sites 1-6 are summarized in Table 3 for a target 25-year level of protection, and an average sea level rise scenario of + 1 m in 2100 with respect to the situation of 2020 (van Berchum et al., 2020). The design wave heights vary between 2.1-3.7 m, and the design water levels between 4.4-5.1 m for a return period of 25 years (IWM,

2018). It should be noted that van Berchum et al. (2020) applied one design condition per polder, whereas different parts of the coastline may have varying wave exposure in terms of fetch, water depth, and coastline angle with respect to the dominant wave direction.

Table 3. Design conditions (surge levels and incoming significant wave heights, H_{m0}) from IWM (2018) and associated embankment crest height from van Berchum et al. (2020) at sites with potential for developing mangrove belts seaward from embankments.

Site number	Polder	Location	Surge [mPWD] 2-M	H_{m0} [m] 2-M	Required crest height [m] 2-M
1	55/4	Galachipa	4,9	3,7	6,3
2	55/3	Galachipa	5,1	2,3	5,9
3	56/57	Bhola	5	3,0	6,1
4	73/2	Hatiya South	4,9	3,4	6,2
5	66/3	Khangona	4,8	2,1	5,5
6	69	Boro Moheshkhali	4,4	2,7	5,4

3.2. Modeling approach

The method to include the effect of mangroves on embankment designs is schematized in Figure 3.2, and consists of the following steps:

- Propagating waves from the offshore boundary to the toe of the structure (Equations 4-6 of Appendix B)
- Estimating potential vegetation failure (Equations 2 and 11-14 of Appendix B)
- Designing embankment using propagated waves as input, specifically:
    - The crest height of the embankment (Equation 7 of Appendix B), and
    - The size of the blocks of the slope (Equation 8 of Appendix B)
- Estimating the shear stresses at the toe of the structure (Equation 9-10 of Appendix B).

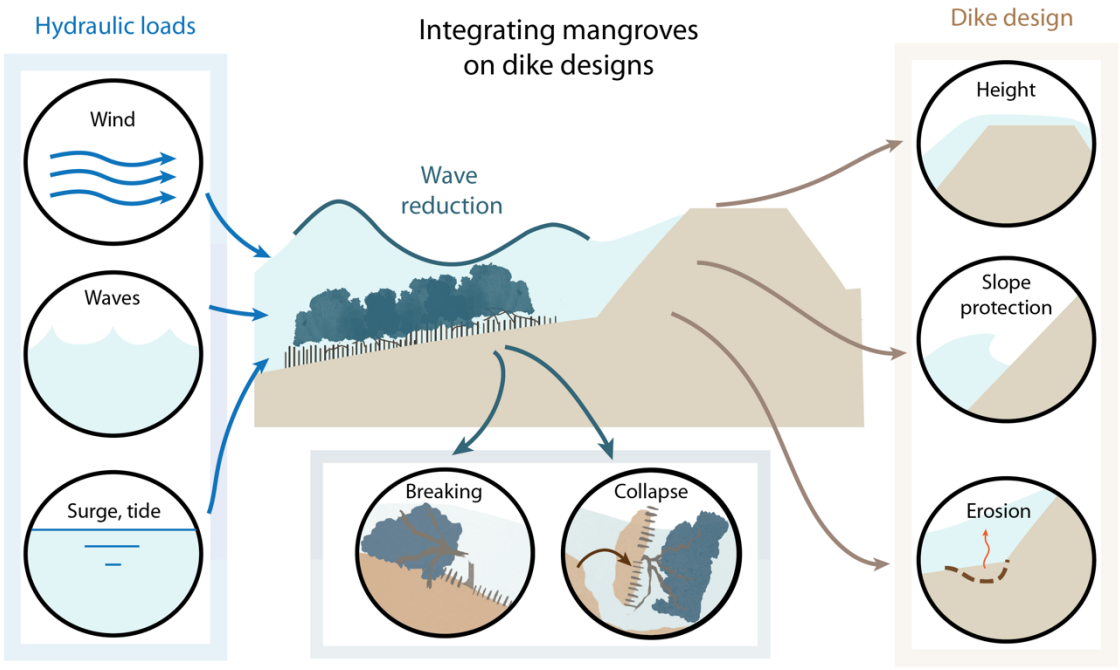

Figure 3.2 Diagram illustrating the modeling approach used to estimate the effect of a mangrove belt on embankment designs. Wave height reduction by mangroves is estimated for different hydraulic conditions and vegetation properties. The effect of wind and waves on tree stability is estimated by comparing the loads acting on the trees with respect to their resistance. Lastly, the wave reduction by the trees is implemented into the embankment design formulas to estimate their effect on the embankment height, on the stone size needed as slope protection, and on the wave-driven shear stresses at the toe of the embankment.

3.3. Modeling scenarios for embankment designs in Bangladesh

The design wave heights and water levels for the modeling scenarios are obtained from the cost-calculation tool of van Berchum et al. (2020) (Table 3). Their study does not specify the wave period associated to each wave height but assumes a wave steepness of $s_0 = 0.05$, where the steepness s_0 is defined as the ratio between the wave height H_{m0} and the wavelength L. The corresponding wavelengths are obtained as $L = s_0/H_{m0}$, and the wave periods are derived using the dispersion relation for linear wave theory with the design water levels. For the bathymetry, schematized linear profiles with slopes between 0.001-0.1 are considered, and the embankment toe is set at an elevation equal to mean high water (MHW).

Wave overtopping over the embankments is estimated using the formula of van der Meer (2018) (Equation 7 in Appendix B). For coastal embankments, we assume slopes of 1:8, armor layers (corresponding with $\gamma_f = 0.55$), and a berm (with $\gamma_b = 0.89$). We also assume

perpendicular wave incidence (so $\gamma_\beta = 1$), and no vertical walls ($\gamma_v = 1$). In each scenario, the crest height of the embankment is adjusted to reach an overtopping rate of 5 l/m/s under design conditions, which is also used in the CEIP-1 design (Government of Bangladesh, 2012). The size of the slope protection is calculated using Equation 8 of Appendix B. The shear stresses at the toe of an embankment are calculated assuming a grain size of $D_{n50} = 7\mu$m in Equations 9-10 of Appendix B.

4. Results

4.1. Wave dissipation by mangroves over time

The wave energy dissipation caused by the different parts of a mangrove tree (canopy, trunk, and roots) is shown in Figure 4.1 (b) as a function of tree age. The energy dissipation is calculated for an offshore wave height of $H_{m0} = 2$ m, and a water level of $h = 5$ m. The drag coefficient and the tree density are set to $c_{D,w} = 1$ and $N_v = 0.1$ trees/m^2, respectively. The model results suggest that the canopy has a significant role in wave dissipation until the trees are 20 years old. Beyond that age, only the trunk and roots contribute wave dissipation, and wave dissipation increases as the roots become wider and taller with age, and as the trunk also enlarges as trees grow older.

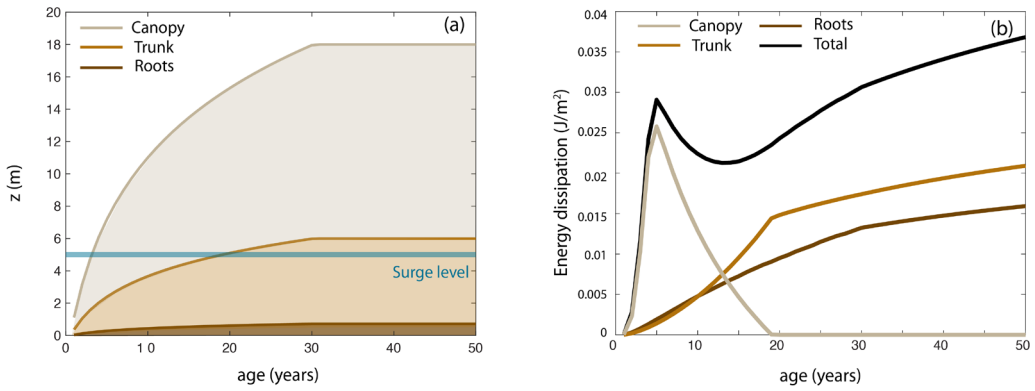

Figure 4.1. (a) Height of the different tree sections (canopy, trunk, and roots) as a function of tree age. (b) Wave energy dissipation by the different tree sections (canopy, trunk, and roots) as a function of tree age.

4.2. Wave attenuation through a mangrove belt

4.2.1. Effect of wave height on wave attenuation

The effect of the incoming wave height on wave attenuation by a 100 m belt with a slope of 1/100 is evaluated for different forest ages in Figure 4.2 for $c_{D,w} = 0.7$ (Figure 4.2 b) and for $c_{D,w} = 1.3$ (Figure 4.2 c). Wave attenuation is here defined as the reduction in wave height at the toe of an embankment with respect to a situation without mangroves:

$$Wave\ attenuation\ (\%) = 100 \frac{H_{no\ veg} - H_{veg}}{H_{no\ veg}} \quad (1)$$

where $H_{no\ veg}$ is the wave height at the embankment toe without mangrove vegetation, and H_{veg} is the wave height at the same location considering the presence of a mangrove foreshore. Without mangroves, waves experience dissipation due to breaking across the bare foreshore. In the presence of mangroves, waves experience additional dissipation due to the resistance exerted by the trees. As it can be seen in Figure 4.2 (b)-(c), young trees below 5-years-old induce attenuation rates smaller than 4% in all scenarios, and wave attenuation increases as trees grow older.

Wave reduction by mangroves also varies with the height of the incoming waves, as the wave height influences both wave breaking and wave dissipation by the vegetation. Higher waves experience more dissipation due to breaking both seaward from and inside the forest. Conversely, smaller waves penetrate further into the forest and experience proportionally more wave attenuation by the vegetation (compared to how much they decrease due to wave breaking). Although the model results provide an indication of the potential wave attenuation provided by the mangroves, the choice of drag coefficient can significantly affect the predictions. For instance, the maximum wave attenuation by a 50-year-old forests increases from 16% to 25% when the drag coefficient is increased from $c_{D,w} = 0.7$ to $c_{D,w} = 1.3$. Wave reduction by mangroves is also very dependent on the vegetation properties, water levels, and profile slope; additional sensitivity analyses are provided in Appendix E.

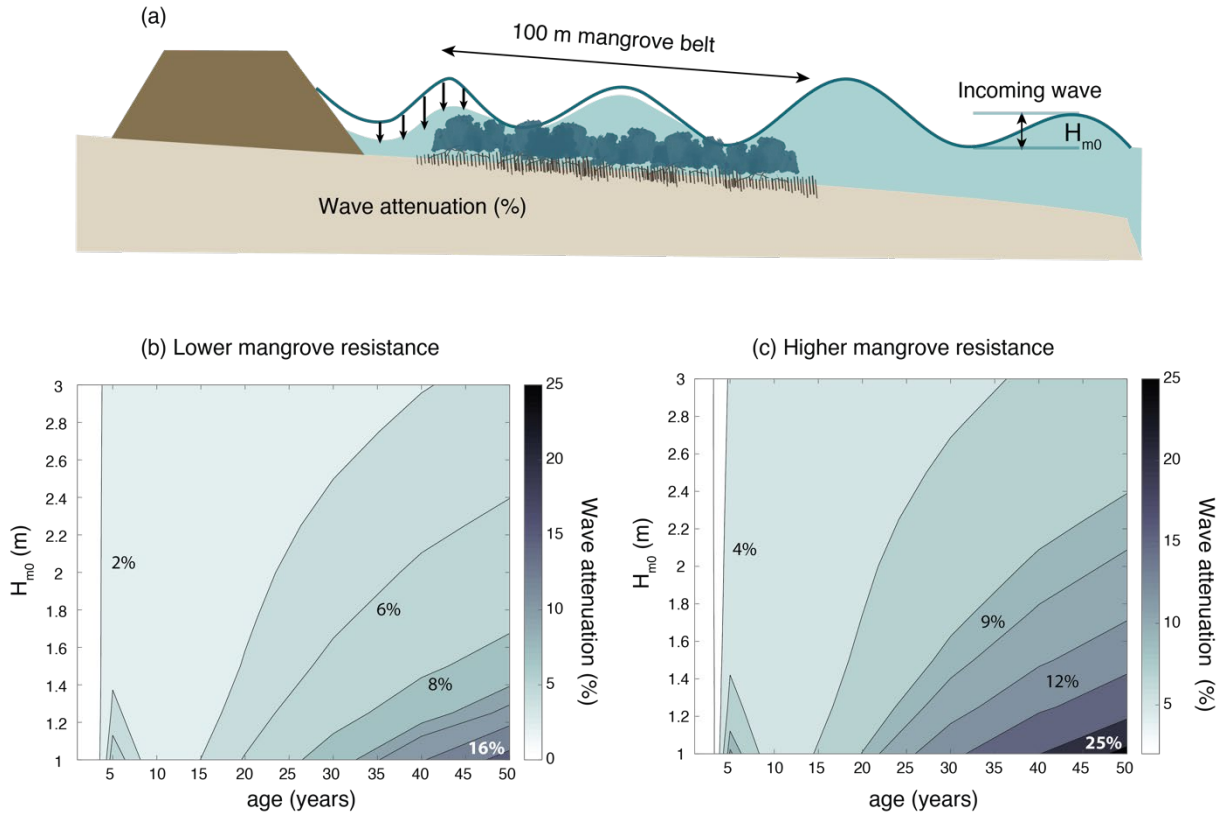

Figure 4.2. (a) Effect of incoming wave height on wave attenuation by a 100 m mangrove belt with respect to a situation without mangroves. Plot (b) corresponds with the geometrical tree model presented in Figure A4, $c_{D,w} = 0.7$ and $N_v = 0.1$ trees/m^2. Plots (c) corresponds with the same tree model and input parameters, except for a larger drag coefficient of $c_{D,w} = 1.3$.

4.2.2. Effect of forest length on wave attenuation

The previous section investigated wave attenuation by a 100 m stretch of mangroves, but wider forests would increase the wave height reduction rates. The effect of the forest length is evaluated in Figure 4.3 for a slope of 1/1000, and two drag coefficients of $c_{D,w} = 0.7$ (Figure 4.3, b) and $c_{D,w} = 2.0$ (Figure 4.3, c). Extending the mangrove belt from a width of 100 m to a width of 1000 m increases wave attenuation by a 50-year-old forest from 7% to 30% with $c_{D,w} = 0.7$, and from 20% to 55% with $c_{D,w} = 2.0$.

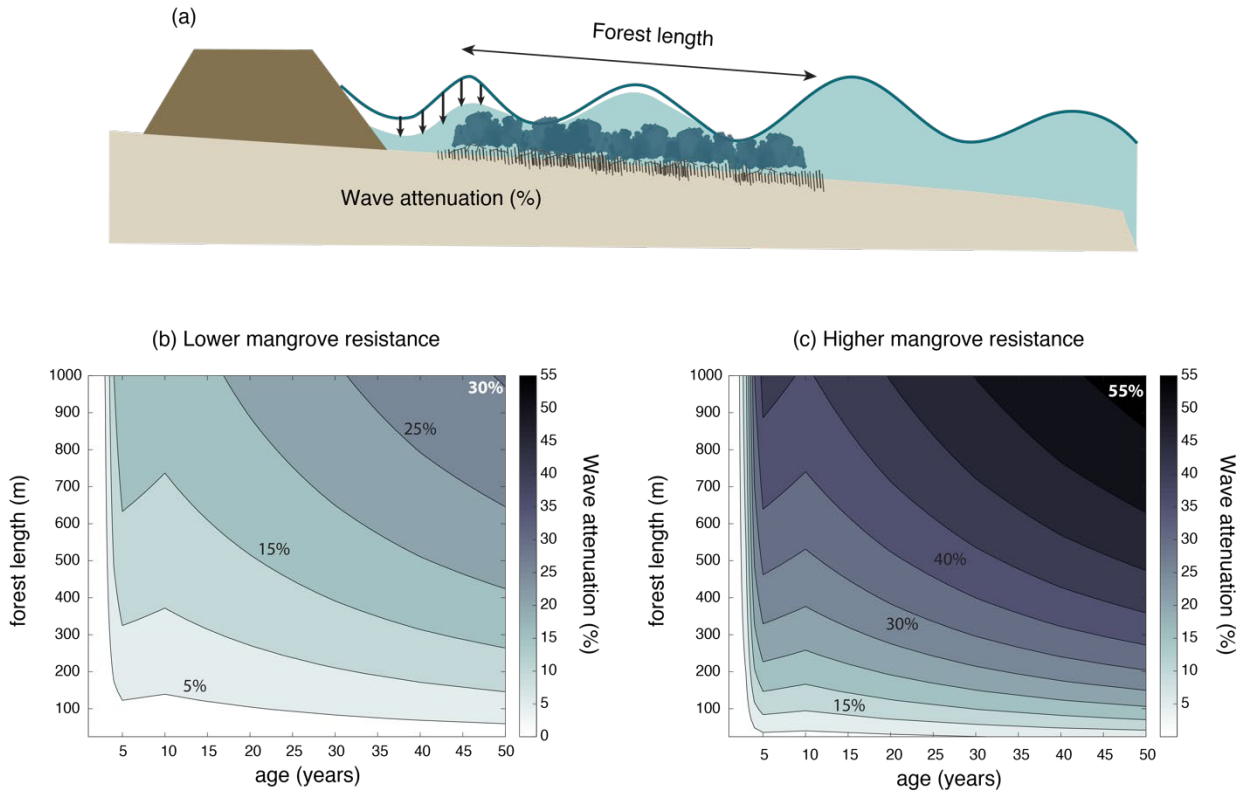

Figure 4.3. (a) Wave attenuation as a function of the forest length. Plot (b) corresponds with the geometrical tree model presented in Figure A4, $c_{D,w} = 0.7$, $N_v = 0.1$ trees/m^2, a slope of 1/1000, $H_{m0} = 2$ m and $h = 5$ m. Plot (c) corresponds with the same modeling parameters except for a higher drag coefficient of $c_{D,w} = 2.0$.

4.3. Vegetation failure

Mangroves can be exposed to both wind and wave loads, as illustrated in Figure 4.4 (a). When trees are very young, they can remain below the water surface during storm events and therefore experience wave loads (Figure 4.4 a). As mangroves grow, they rise above the water surface and the total forces acting on them are dominated by the effect of the wind. For trees that are partly submerged, the wind loads are much larger than the wave loads (Figure 4.4, b), since the tree canopy constitutes a large part of the tree area, and because the modeled wind speed causes relatively larger forces than the wave velocities (even if air has a lower density, as discussed in Section 2.3).

The bending moment associated to wind and wave forces is shown in Figure 4.4 (c) and compared with the maximum bending moment for trunk breakage and for tree overturning.

The bending moment acting on the trees is governed by the contribution of the wind, as both the force and the arm are relatively larger for wind loads. The resistance for overturning is exceeded for both trees at the seaside (Figure 4.4, c) and land side of the forest (Figure 4.4, d). Although a tree placed at the landward side of the mangrove belt experiences more wind attenuation inside the canopy (Equation 13 in Appendix B) it is exposed to a larger bending moment. This higher vulnerability is caused by the behavior of the empirical gust factor G, which increases with the distance from the forest edge (Equation 14 in Appendix B).

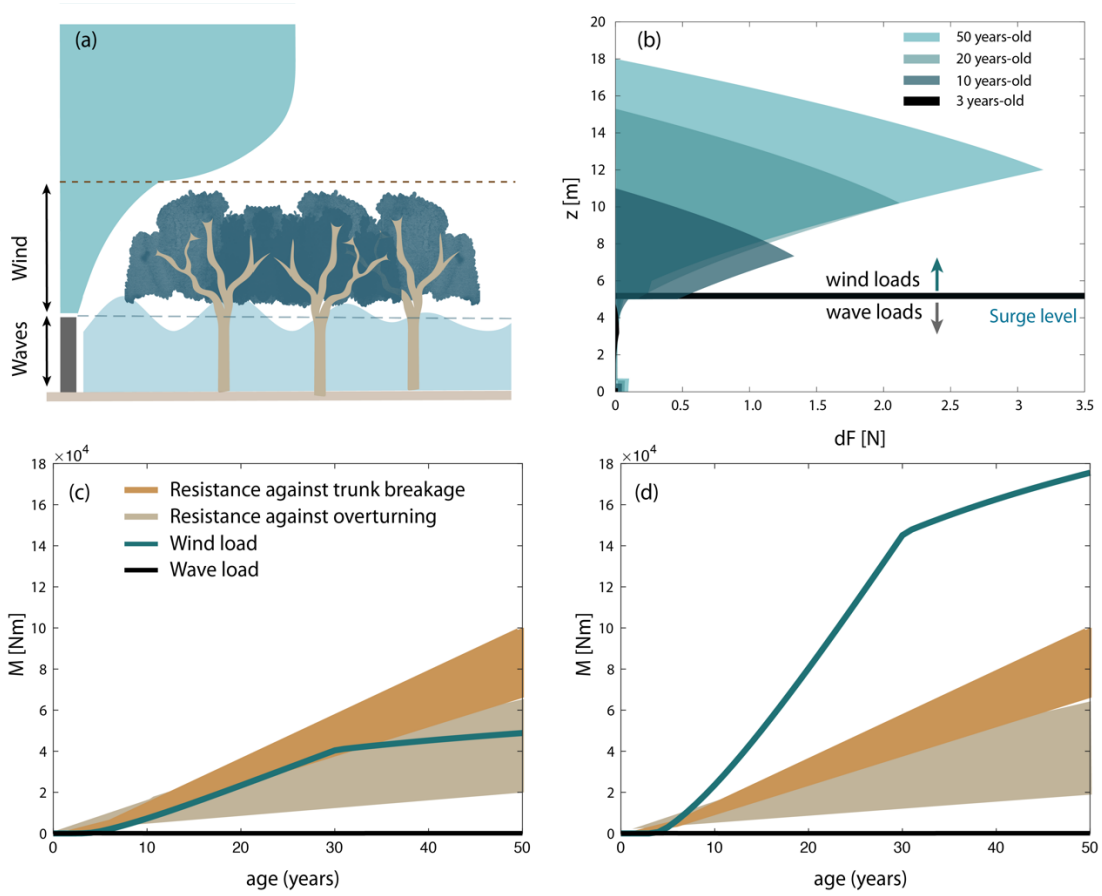

Figure 4.4. (a) Schematic representation of the loads acting on mangrove trees, consisting of wave loads (acting on the submerged area) and wind loads (acting on the emerged area). (b) Modeled forces acting on a mangrove tree placed at the seaward edge of a mangrove belt during a cyclone with wind speeds of 120 km/h. In the model runs, $c_{D,w} = 1$, $c_{D,c} = 1$, $c_M = 1$, $N_v = 0.1$ *trees/m²,* $slope = 1/1000$, $H_{m0} = 2$ m and $h = 5$ m. *The lower plots show the overturning moment acting on a mangrove tree placed on the (c) seaward side of the mangrove belt, and on the (d) landward side of the mangrove belt. The brown lines and areas show the vegetation limits against trunk breakage (dark brown) and tree overturning (light brown).*

4.4. Effect of wave attenuation on structure designs

4.4.1. Embankment height

The effect of a mangrove belt on the embankment height is shown as a function of the forest age in Figure 4.5 (b), and as a function of the forest length in Figure 4.5. (c). Figure 4.5 (b) suggests that the effect of mangroves on the embankment height is only appreciable after 15 years from initial mangrove establishment. However, the required embankment height is also lower in the beginning of the structure lifetime (see blue line in Figure 4.5, b), and it increases over time with rising sea levels. This implies that the vegetation is most efficient in reducing the design water levels when it is also most necessary. However, for the modeled conditions (and generally for the boundary conditions of Table 3) the required embankment height is mostly determined by the surge level. A mangrove belt of 100 m has a relatively small effect on the structure height, which can be reduced in 0.09 m with respect to a situation without mangroves (Figure 4.5 c). Wider mangrove foreshores increase wave dissipation by both wave breaking and by the resistance exerted by the vegetation. A mangrove belt of 1000 m can therefore reduce the embankment height in 30 cm (with respect to a situation with a bare profile), but this value is also small compared to the total embankment height. Figure 4.5 (c) also suggests that this height reduction is mostly achieved by the first 500 m of the forest, whereas incrementing the forest width beyond this value has a relatively smaller effect on the crest height.

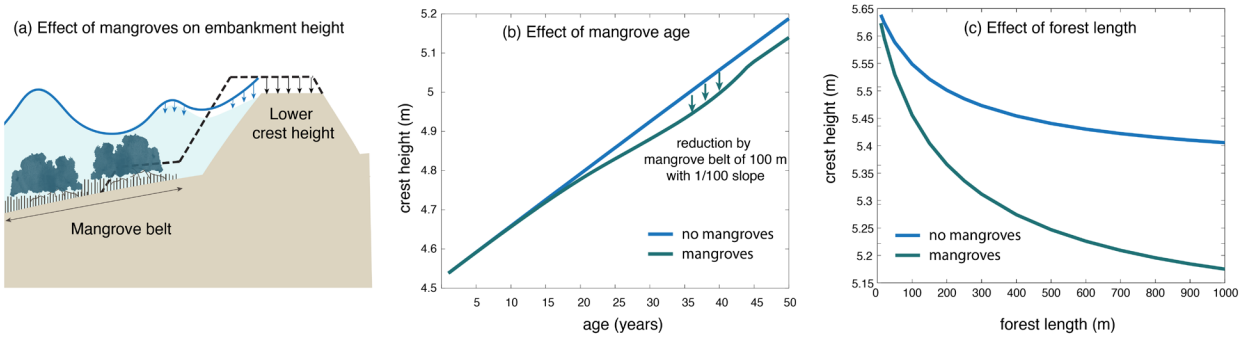

Figure 4.5. (a) Schematic picture showing the effect of mangroves on the embankment height. (b) Effect of mangroves on the embankment crest height as a function of the forest age for a 100 m stretch of mangroves over a profile with a slope of 1/100. (c) Effect of forest length on the embankment crest height for a slope of 1/1000. The results of (b)-(c) correspond with an offshore wave height of 2 m. The vegetation properties in plots (b)-(c) correspond with the tree model presented in Figure A4. In the runs and, $c_{D,w} = 1.3$, $N_v = 0.1$ *trees/m*^{2}, $H_{m0} = 2$ m and $h = 5$ m.

4.4.2. Slope protection

Wave attenuation by a mangrove belt also decreases the wave loads acting on embankment slopes, and their protection needs. The effect of mangroves on the required slope protection (Figure 4.6) is more pronounced than on the crest height (Figure 4.5). At a coastal profile with a slope of 1/1000, a mangrove stretch with a width of 100 m reduces the thickness of the slope protection blocks by 13% (Figure 4.6, b), and a wider forest with a size of 1000 m could decrease their thickness by 46% (Figure 4.6, b) for a wave height of 2 m and a surge level of 5 m.

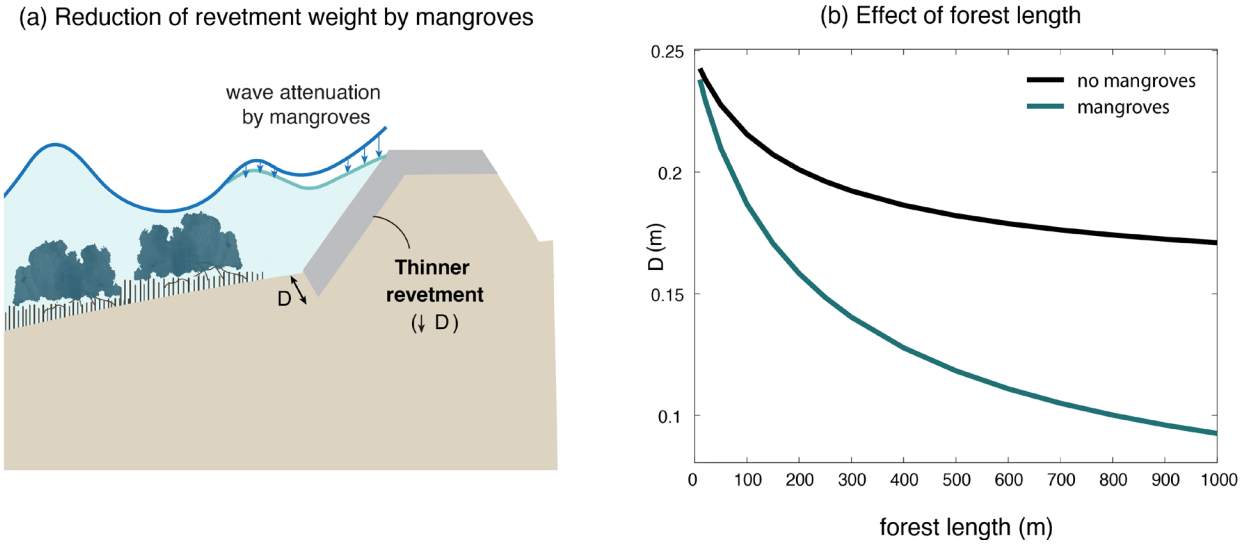

Figure 4.6. (a) Diagram illustrating how wave attenuation by mangroves can reduce the required thickness of the slope protection blocks. (b) Effect of the forest length on the revetment thickness reduction for a profile with a slope of 1/1000 and a surge level of 5 m at the toe of the embankment. The mangrove properties of plot (b) correspond with the tree model presented in Figure A4. In the runs, $c_{D,w} = 1.3$ and, $N_v = 0.1$ trees/m^2, and the offshore wave height is equal to 2 m.

4.4.3. Shear stresses at the toe of the embankment

Mangroves can also have a significant effect on the shear stresses. At a coastal profile with a slope of 1/1000, a mangrove stretch with a width of 100 m can already reduce the shear stresses by 25% (Figure 4.7, b), and a wider forest with a size of 1000 m could decrease them by 70% (Figure 4.7, b) for a wave height of 2 m and a surge level of 5 m.

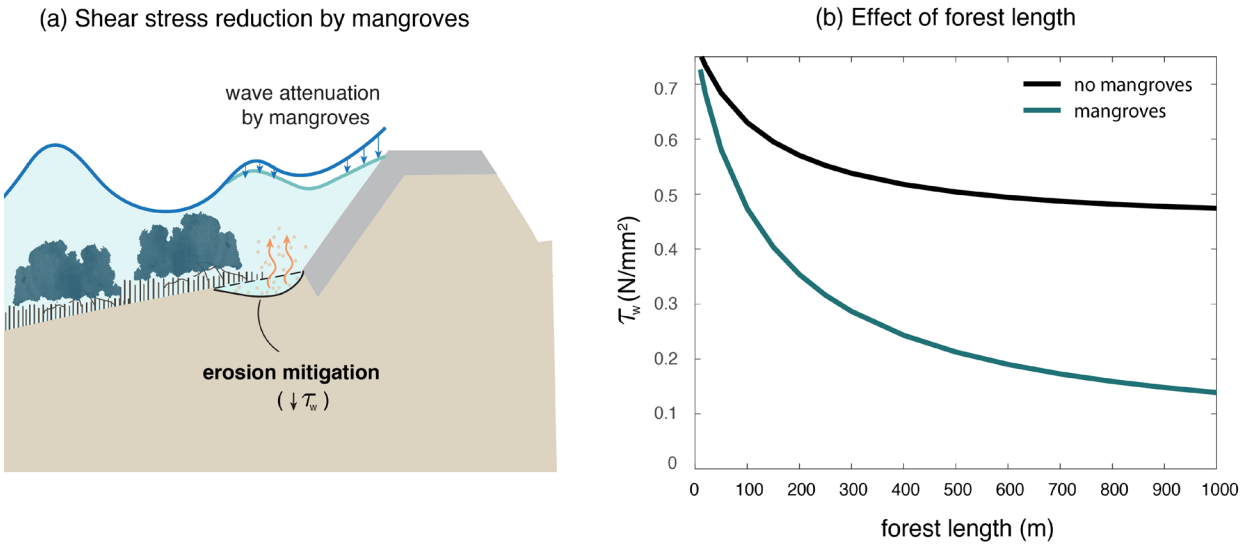

Figure 4.7. (a) Diagram illustrating how wave attenuation by mangroves can reduce the shear stresses at the toe of an embankment. (b) Effect of the forest length on the shear stresses for a profile with a slope of 1/1000 and a surge level of 5 m at the toe of the embankment. The mangrove properties of plot (b) correspond with the tree model presented in Figure A4. In the runs, $c_{D,w} = 1.3$ *and,* $N_v = 0.1$ *trees/m*^{2}*, and the offshore wave height is equal to 2 m.*

4.5. Potential effect of mangroves at afforestation sites

The effect of developing a mangrove belt of 100 m at the potential afforestation sites of Table 3 is summarized in Table 4. The presence of the mangrove belt could reduce the wave-driven shear stresses by 15-23%, which in turn would decrease the erosion rates and scour at the toe. Such mangrove belt could also reduce the required thickness of the slope protection by 8%-12%. Lastly, mangroves could decrease the required embankment height in approximately 0.06-0.09 m for the design conditions of Table 3.

Table 4. Estimated effect of mangroves at the potential afforestation sites summarized in Table 3. For each case, the effect of a 100-m wide mangrove belt with a slope of 1/100 is evaluated in terms of (1) embankment height reduction, (2) reduction of the thickness needed for slope protection, and (3) reduction of the shear stresses at the toe of the embankment. The estimates are obtained for $c_{D,w} = 1.3$, $N_v = 0.1$ trees/m^2, and a profile slope of 1/100.

Site number	Polder	Location	Surge [mPWD] 2-M	H_{m0} [m] 2-M	100 m of mangroves with slope of 1/100		
					Crest height reduction [m]	Slope protection reduction [%]	Stress reduction [%]
1	55/4	Galachipa	4,9	3,7	0.08	8	15
2	55/3	Galachipa	5,1	2,3	0.09	11	21
3	56/57	Bhola	5	3	0.08	9	17
4	73/2	Hatiya South	4,9	3,4	0.08	8	16
5	66/3	Khangona	4,8	2,1	0.09	12	23
6	69	Boro Moheshkhali	4,4	2,7	0.06	8	16

A wider belt of 500 m over a shallower profile with a slope of 1/1000 would have a more pronounced effect on embankment designs (Table 5) with a crest height reduction of 0.13-0.19 m, a slope protection thickness reduction of 23%-32%, and a shear stress reduction of 41%-54%. It should be noted that these predictions are indicative of the potential effect of afforesting mangrove belts, but they are highly sensitive to the choice of vegetation properties and drag coefficient. More accurate predictions could be obtained by using the geometric and mechanical properties of the local mangrove species (see Section 5).

Table 5. Estimated effect of mangroves at the potential afforestation sites summarized in Table 3. For each case, the effect of a 500-m wide mangrove belt with a slope of 1/1000 is evaluated in terms of (1) embankment height reduction, (2) reduction of the thickness needed for slope protection, and (3) reduction of the shear stresses at the toe of the embankment. The estimates were obtained for $c_{D,w} = 1.3$, $N_v = 0.1$ trees/m^2, and a profile slope of 1/1000.

Site number	Polder	Location	Surge [mPWD] 2-M	H_{m0} [m] 2-M	500 m of mangroves with slope of 1/1000		
					Crest height reduction [m]	Slope protection reduction [%]	Stress reduction [%]
1	55/4	Galachipa	4,9	3,7	0.16	23	41
2	55/3	Galachipa	5,1	2,3	0.19	31	53
3	56/57	Bhola	5	3	0.17	26	45
4	73/2	Hatiya South	4,9	3,4	0.16	24	42
5	66/3	Khangona	4,8	2,1	0.18	32	54
6	69	Boro Moheshkhali	4,4	2,7	0.13	24	42

5. Discussion

Model limitations

The geometric tree model applied in this study is a conservative representation of real trees, especially regarding the total canopy surface. Since the canopy area is determined from photographs, overlapping branches are not included in the area estimates. Moreover, small branches are neglected in Section 4, and the effect of leaves is also disregarded in the analysis under the assumption that leaves are quite flexible and easily detachable for *S. apetala* trees (van Hespen et al., 2021). Despite their flexibility, these elements likely contribute to some extent to wave dissipation by the trees.

Besides the underestimation of the tree area, in most runs the drag coefficients are not increased above $c_{D,w} = 1.3$ even though the drag coefficient estimates of van Hespen et al. (2021) for *S. apetala* branches reach values between of $c_{D,w} = 2 - 6$. As discussed in Appendix D, $c_{D,w}$ values above 2.5 exceed the expected drag range for cylindrical elements, and such overprediction could be due to a combination of scale effects and due to testing single branches in isolation. The values between $c_{D,w} = 0.7$-1.3 used in most runs are relatively more conservative and would be representative of situations with sheltering and/or where plant flexibility reduces wave dissipation by the trees. Values larger than $c_{D,w} = 1.3$ would also be possible in the field, and scenarios with $c_{D,w} = 2$ show almost 50% more wave attenuation than those obtained with $c_{D,w} = 0.7$ (Figure 4.3 b-c). Such large differences suggest that good predictions of $c_{D,w}$ are key for precise assessments of the effect of mangroves.

With respect to vegetation damage, only two failure mechanisms (overturning and trunk breakage) are considered in this paper, whereas trees can die due to other causes such as pests, massive leaf loss, burial, uprooting, and hyper salinity. For tree overturning, maximum resistance values for terrestrial trees were used, whereas the maximum bending moment is likely to depend on the local soil and mangrove properties. The wave attenuation predictions are not updated to account for tree failure, which implies that the wave attenuation rates may be overpredicted for the most extreme wave conditions.

Implementing mangroves in embankment designs

Although the present study indicates that 100-m belts of *S. apetala* could have an appreciable effect on embankment designs, a narrow forest with a single mangrove species would be highly vulnerable to pests and have an overall lower resilience against extreme events. Our modeling work suggests that wind loads could exceed the tree resistance of *S. apetala* mangroves for wind speeds of 120 km/h, which on average hit the coast of Bangladesh every 3 years (Dasgupta et al., 2017). Tree pruning could be a potential method to reduce the loads acting on the trees, and this option could be investigated in future studies. Moreover, other pioneer species like *A. officinalis* could also be relatively more stable than *S. apetala* trees for potential afforestation sites.

Since different mangrove species grow at different ground elevations with respect to MSL, a more biodiverse forest requires a wider extension than a plantation with a single species. Wider forests would also provide an additional buffer during situations in which part of the forest is damaged. The choice of the optimal mangrove width is site-specific and requires balancing several factors such as the ecological requirements for mangrove establishment and survival, the potential flood risk reduction by the vegetation, and the costs and benefits of other alternatives (such using the land for other purposes). Climate change may be another important consideration for species selection, as increasing inundation and salinity may reduce the long-term survival of some species (Dasgupta et al., 2017b; Mukhopadhyay et al., 2018).

Another important consideration for design implementations is that mangroves need time to grow, and their wave attenuation efficiency increases over time. However, embankments also experience increasing design water levels and wave loads with time due to sea level rise. The embankment height can also progressively reduce due to processes like subsidence or compaction of the earth filling. Assuming that maintenance works must be done when the height of a structure reaches a minimum threshold value (due to ground sinking or

compaction), the presence of mangroves could reduce the frequency of maintenance works, as illustrated in Figure 5.1 (a).

Alternatively, embankments could be designed with a lower initial height and a thinner slope revetment accounting for the presence of mangroves. In both cases, frequent monitoring would be essential to ensure that mangroves are developing as expected, and to identify any potential damage by storms or pests. Since the evolution of a mangrove belt is very sensitive to the local morphodynamics, and to the ecology of the local species, it is recommended to conduct pilot studies where mangroves planted seaward from embankments, monitor their evolution, and use the monitoring data to optimize future designs. For a pilot, the strategy shown in Figure 5.1. (a) could be implemented to explore the potential of having a mangrove foreshore without compromising the safety of the hinterland.

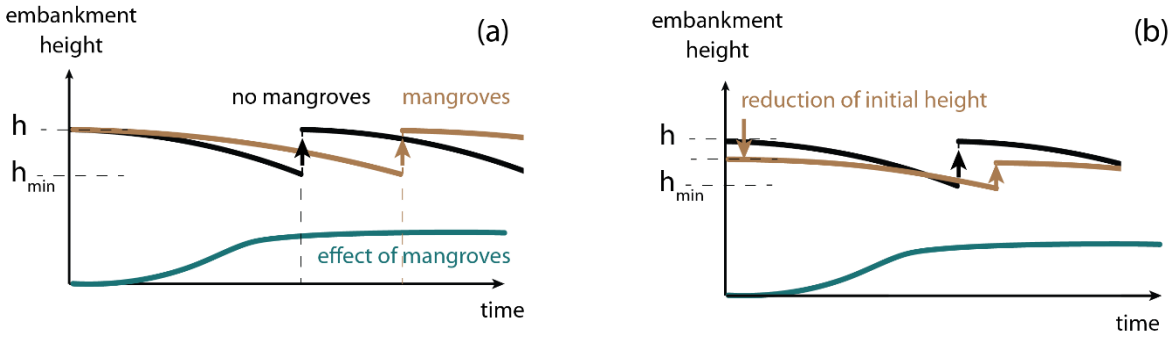

Figure 5.1. Effect of mangrove implementation on reinforcement works. (a) Situation where the same embankment height is implemented with and without mangroves. Over time, the vegetation will grow and the wave attenuation that it produces will reduce the design water levels on the embankment. As the embankment filling compacts or the ground subsides, the vegetation could compensate the reduction in structure height, and maintenance works could be done with a lower frequency. (b) Alternatively, the initial height of the embankment could be reduced, taking into consideration that the mangroves can partly compensate the height reduction and the effect of sea level rise. In both cases, frequent monitoring would be necessary to ensure the safety levels are met.

Lastly, this paper focuses on the effect of mangroves on waves, but a mangrove belt would also influence other physical processes related to embankment designs. For instance, we analyze how vegetation would reduce wave-driven shear stresses during cyclones, while current-driven shear stresses are not considered in this study. However, Dasgupta et al. (2017) reported potential current reduction rates by mangroves during cyclones between 33%-85%, which would mitigate damages on the slope and bank protection of embankments.

Mangroves could also affect the morphology of the foreshore, further reducing wave attack on the embankments. Such processes could be investigated with morphodynamic models, and, as previously suggested, be monitored over the life of the structures.

6. Conclusions

This paper investigates the potential wave load reduction by mangroves on coastal embankments in Bangladesh. The main conclusions of this study are listed below:

- Mangrove belts with widths between 100-1000 m could attenuate waves up to 7%-55% with respect to the situation without mangroves (for a forest age of 50 years-old).
- Such wave attenuation rates would reduce embankment heights in approximately 0.09-0.30 m, decrease the thickness of the slope protection by 13%-46% and reduce the shear stresses at the toe of the embankment by 25%-70% for the design conditions of the embankments.
- Although 100-m belts of *S. apetala* mangroves already show an appreciable effect on embankment designs, such narrow belts would be quite vulnerable to extreme conditions and could be largely damaged by pests. Wider forests with higher biodiversity are recommended to provide extra safety against extreme events and to increase their resilience.

7. Recommendations

To reduce the uncertainty in the modeling results, the following steps are recommended:

- Collecting data of the local mangrove pioneers, particularly of their geometry and stability as a function of tree age.
- Measuring wave attenuation through mangrove belts in Bangladesh, to collect validation data for the wave model.
- Quantifying morphodynamic effects of the mangrove vegetation on the coastal profile.
- Conducting and monitoring pilot studies where mangroves are planted seaward from embankment and collecting data for the optimization of future designs.

8. References

Alongi, D.M. (2002). Present state and future of the world's mangrove forests. Environ. Conserv. 29, 331–349.

Awal, M.A.; Islam, A.F.M. (2020). Water Logging in south-western coastal region of Bangladesh: Causes and consequences and people's response. Asian J. Geogr. Res, 3, 9–28.

Best, Ü.S.N., Van der Wegen, M., Dijkstra, J., Willemsen, P.W.J.M., Borsje, B.W., Roelvink, D.J.A., (2018). Do salt marshes survive sea level rise? Modelling wave action, morphodynamics and vegetation dynamics, Environmental Modelling & Software 109: 152-166,

Bao, T. (2011). Effect of mangrove forest structures on wave attenuation in coastal Vietnam. Oceanologia. 76. 10.5697/oc.53-3.807.

Bhowmik, A., Cabral, P. (2013). Cyclone Sidr Impacts on the Sundarbans Floristic Diversity. Earth Science Research. 2. 62-79. 10.5539/esr.v2n2p62.

Bricheno, L.M., Wolf, J., Islam, S., (2016). Tidal intrusion within a mega delta: An unstructured grid modelling approach. Estuarine, Coastal and Shelf Science 182, 12-26.

Carrol, C.A., Bunting, P., Hardy, A., Bell, G. (2019). Using Continuous Change Detection and Classification of Landsat Data to Investigate Long-Term Mangrove Dynamics in the Sundarbans Region. Remote Sens. 2019, 11(23), 2833; https://doi.org/10.3390/rs11232833

Dasgupta, S., Huq, M., Khan, Z.H., Zahid Ahmed, M.M, Mukherjee, N., Khan, M.F., Pandey, K. (2014). Cyclones in a changing climate: the case of Bangladesh, Climate and Development, 6:2, 96-110, DOI: 10.1080/17565529.2013.868335

Dasgupta, S., Islam, M.S., Huq, M., Khan, Z.H., Hasib, M.R. (2017). Mangroves as Protection from Storm Surges in Bangladesh. Policy Research Working Paper 8251.

Dasgupta, S., Sobhan, I., & Wheeler, D. (2017b). Impact of Climate Change and Aquatic Salinization on Mangrove Species in the Bangladesh Sundarbans. Vol. 46, No. 6, 680-694.

Eckstein, D., Künzel, V., Schäfer, L., Winges, M. (2020). Global Climate Risk Index 2019. Germanwatch e.V.

Etminan, V., Lowe, R., Ghisalberti, M., 2019. Canopy resistance on oscillatory flows. Coast. Eng. 152 https://doi.org/10.1016/j.coastaleng.2019.04.014.

Gardiner, B. A., G. R. Stacey, R. E. Belcher, and Wood, C. J. (1997). Field and wind-tunnel assessment of the implications of respacing and thinning on tree stability. Forestry 70:233-252.

Gardiner, B.A., Berry, P., Moulia, B. (2016). Review: Wind impacts on plant growth, mechanics and damage. Plant Science 245.

Gijón Mancheño, A., Herman, P.M.J., Jonkman, S.N., Kazi, S., Urrutia, I., van Ledden, M. (2021). Mapping mangrove opportunities with open access data: A case study for Bangladesh. Sustainability 13.

Global Forest Watch (2020). https://www.globalforestwatch.org

Government of Bangladesh (2012). Detailed design of 5 polders. Volume I. Design report.

Herrera-Silveira, J. A., Teutli-Hernandez, C., Secaira-Fajardo, F., Braun, R., Bowman, J., Geselbracht, L., Musgrove, M., Rogers, M., Schmidt, J., Robles-Toral, P. J., Canul-Cabrera, J. A., & Guerra-Cano, L. (2022). Hurricane Damages to Mangrove Forests and Post-Storm Restoration Techniques and Costs. The Nature Conservancy, Arlington, VA.

Horstman, E., Dohmen-Janssen, M., Narra, P., Van den Berg, N.J., Siemerink, Martijn., Hulscher, S. (2014). Wave attenuation in mangroves: A quantitative approach to field observations. Coastal Engineering. 94. 47–62. 10.1016/j.coastaleng.2014.08.005.

Iftekhar, M.S., Islam, M.R. (2004) Degeneration of Bangladesh Sundarbans mangroves: a management issue. Int Forest Rev 6:123–135

Iftekhar, M.S., Saenger, P. (2008). Vegetation dynamics in the Bangladesh Sundarbans mangroves: a review of forest inventories. Wetlands Ecol Manage 16: 291–312.

IPCC (2007). Climate Change 2007: Impacts, Adaptation and Vulnerability: Summary for Policymakers. Working Group II Contribution to the Intergovernmental Panel on Climate Change Fourth Assessment Report. IPCC, Geneva.

Islam, S.A., Bala, S.K., Hussain, M.A., Rahman, M.M. (2011). Performance of Coastal Structures during Cyclone Sidr. Natural Hazards Review 12(3).

Islam, S.A., Miah, S.A.Q., Habib, M.A., Alam, M.M. (2016). Growth and yield of Sonneratia apetala (keora) plantations raised from different seed sources in the central coastal belt of Bangladesh. Journal of Bioscience and Agriculture Research 6.

IWM (2018). Technical Report on Storm Surge, Wave, Hydrodynamic Modelling and Design Parameters on Drainage System and Embankment Crest Level. Volume-II: Package 2 (Appendix B: Storm Surge). Bangladesh Water Development Board, Ministry of Water Resources.

Jakobsen, F., Zeaul Hoque, A.K.M., Paudyal, G.N., Bhuiyan, Md. S., (2005) Evaluation of the Short-Term Processes Forcing the Monsoon River Floods in Bangladesh, Water International, 30:3, 389-399, DOI: 10.1080/02508060508691880

Jiang, Z., Guan, W., Xiong, Y., Li, M., Chen, Y., Liao, B., (2019). Interactive Effects of Intertidal Elevation and Light Level on Early Growth of Five Mangrove Species under Sonneratia apetala Buch. Hamplantation Canopy: Turning Monocultures to Mixed Forests. Forests, 10(2), 83.

Kaimal, J.C., Finnigan, J.J. (1994). Atmospheric Boundary Layer Flows: Their Structure and Measurement. 1st ed., Oxford University Press, New York.

Kalloe, S.A., Hofland, B., Antolínez, J.A., van Wesenbeeck, B.K. (2022). Quantifying Frontal-Surface Area of Woody Vegetation: A Crucial Parameter for Wave Attenuation. Frontiers in Marine Science 23.

Kathiresan, K., Rajendran, N. (2005). Coastal mangrove forests mitigated tsunami. Estuarine, Coastal and Shelf Science. Volume 65, Issue 3, November 2005, Pages 601-606

Keulegan, G.H., Carpenter, L.H., (1958). Forces on cylinders and plates in an oscillating fluid. J. Res. Natl. Bur. Stand. 60, 423–440

Khan, R.S. (1992). Cyclone Hazard in Bangladesh. Community Development library, Dhaka, 86–102. National States Geographic Information Council. Available online: www.adpc.net.

Krauss, K.W.; Doyle, T.W.; Doyle, T.J.; Swarzenski, C.M.; From, A.S.; Day, R.H.; Conner, W.H. (2009). Water level observations in mangrove swamps during two hurricanes in Florida. Wetlands, 29, 142–149.

Lewis III, R.R. (2009). Methods and criteria for successful mangrove forest restoration. In: Gerardo M. E. Perillo, Eric Wolanski, Donald R. Cahoon, Mark M. Brinson, editors, Coastal Wetlands: An Integrated Ecosystem Approach. Elsevier, 2009, p. 787. ISBN: 978-0-444-53103-2

Lewis, R.R., Brown, B. (2014) Ecological mangrove rehabilitation – a field manual for practitioners. Version 3. Mangrove Action Project Indonesia, Blue Forests, Canadian International Development Agency, and OXFAM. p 275.

Lopez-Portillo, J.L., Lewis III, R.R., Saenger, P., Rovai, A.S (2017). Mangrove Forest Restoration and Rehabilitation. Mangrove Ecosystems: A Global Biogeographic Perspective. Springer, Cham. https://doi.org/10.1007/978-3-319-62206-4_10.

Lovelock, C., Cahoon, D., Friess, D., Guntenspergen, G., Krauss, K., Rogers, R., et al. (2015). The vulnerability of Indo-Pacific mangrove forests to sea-level rise. Nature 526

Massel, S.R., Furukawa, K., and Brinkman, R.M. (1999). Surface wave propagation in mangrove forests. Fluid Dynamics Research 24 219.

Maza, M., Lara, J.L., Losada, I. (2021). Predicting the evolution of coastal protection service with mangrove forest age. Coastal Engineering, 168.

Mazda, Y., Wolanski, E., King, B. (1997). Drag force due to vegetation in mangrove swamps. Mangroves and Salt Marshes 1, 193–199. https://doi.org/10.1023/A:1009949411068

McIvor, A., Möller, I., Spencer, T., Spalding, M. (2012) Reduction of wind and swell waves by mangroves. Natural coastal protection series: Report 1. Cambridge coastal research unit working paper 40. The nature conservancy, Arlington, USA/Wetlands International, Wageningen, Netherlands, pp 27

McKee, K. and Vervaeke, W. (2018). Will fluctuations in salt marsh–mangrove dominance alter vulnerability of a subtropical wetland to sea-level rise? Global Change Biology 28

Menéndez, P., Losada, I.J., Torres-Ortega, S., Narayan, S., Beck, M. (2020). The global flood protection benefits of mangroves. Scientific Reports, 10.

Méndez, F.J., Losada, I.J. (2004). An empirical model to estimate the propagation of random breaking and nonbreaking waves over vegetation fields. Coastal Engineering 51(2):103-118

Montgomery, J.M.; Bryan, K.R.; Horstman, E.M.; Mullarney, J.C. (2018) Attenuation of Tides and Surges by Mangroves: Contrasting Case Studies from New Zealand. Water, 10, 1119.

Morison, J. R., Johnson, J.W., O'Brien, M.P. (1950). The force exerted by surface waves on piles. Petroleum Trans. 189, pp. 149–157.

Mukhopadhyay, A., Wheeler, D., Dasgupta, S., Dey, A., Sobhan, I. (2018). Aquatic Salinization and Mangrove Species in a Changing Climate: Impact in the Indian Sundarban. World Bank Policy Research Working Paper No. 8532.

Naz, F.; Buisson, M.C. (2015). Multiple actors, conflicting roles and perverse incentives: The case of poor operation and maintenance of coastal polders in Bangladesh. In Proceedings of the CPWF, GBDC, WLE Conference on Revitalizing the Ganges Coastal Zone: Turning Science into Policy and Practices, Dhaka, Bangladesh, 21–23; pp. 147–161.

Nicholls, R.J., Hoozemans, F.M.J, Marchand, M., (1999). Increasing flood risk and wetland losses due to global sea-level rise: regional and global analyses. Global Environmental Change 9: 69-87.

Nicoll, B.C., Gardiner, B.A., Rayner, B., Peace, A.J. (2006) Anchorage of coniferous trees in relation to species soil type, and rooting depth, Can. J. For. Res. 36. Pp. 1871–1883.

Nishat, A., (1988). Review of present activities and state of art of the coastal areas of Bangladesh. Coastal area resource development and management Part II, pp. 23-35. Dhaka, Coastal Area Resource Development and Management Association (CARDMA).

Pendleton, L., Donato, D. C., Murray, B. C., Crooks, S., Jenkins, W. A., Sifleet, S., Craft, C., Fourqurean J., Kauffman, J., Marbà, N., Megonigal, P.,Pidgeon, E., Herr, D., Gordon, D., and Baldera, A. (2012). Estimating global "blue carbon" emissions from conversion and degradation of vegetated coastal ecosystems. PLoS ONE 7(9): e43542.

Pilarczyk, K.W., (editor) (1990). Coastal Protection, Published by A.A. Balkema, Rotterdam.

Pilarczyk, K.W., (editor) (1998). Dikes and revetments, Published by A.A Balkema, Rotterdam.

Quartel, S., Kroon, A., Augustinus, P., Santen, P., Tri, N.H. (2007). Wave attenuation in coastal mangroves in the Red River Delta, Vietnam. Journal of Asian Earth Sciences. 29. 576-584. 10.1016/j.jseaes.2006.05.008.

Quine, P. and Gardiner, B.A. (2007). Understanding how the interaction of wind and trees results in windthrow, stem breakage and canopy gap formation. Plant Disturbance Ecology.

Rahman, M., Sass-Klaassen, U., Zuidema, P.A., Chowdhury, M.Q., Beeckman, H. (2020). Salinity drives growth dynamics of the mangrove tree Sonneratia apetala Buch. -Ham. in the Sundarbans, Bangladesh. Dendrochronologia, 62.

Rahman, M., Donoghue, D.N.M., Bracken, L.J., Mahmood, H. (2021). Biomass estimation in mangrove forests: a comparison of allometric models incorporating species and structural information. Environmental Research Letters 16.

Rennel, J. (1786). Bengal, Bahar, Oude, Allahabad. General Atlas.

Rivera-Monroy, V.H., Twilley R.R., Mancera-Pineda J.E., Madden C.J., Alcantara-Eguren A., Moser, Jonsson, B.F., Castañeda-Moya, E., Casas-Monroy, O., Reyes-Forero, P., and Restrepo, J. (2011). Salinity and Chlorophyll a as Performance Measures to Rehabilitate a Mangrove-Dominated Deltaic Coastal Region: the Ciénaga Grande de Santa Marta–Pajarales Lagoon Complex, Colombia. Estuaries and Coasts 34, pp. 1-19.

Rudnicki, M., Mitchell, S.J., Novak, M.D. (2004). Wind tunnel measurements of crown streamlining and drag relationships for three conifer species, Can. J. For. Res. 34. Pp. 666–676.

Saintilan, N., Khan, N.S., Ashe, E., Kelleway, J.J., Rogers, K., Woodroffe, C.D., Horton, B.P. (2020). Thresholds of mangrove survival under rapid sea level rise. Science 368.

Saenger, P., Siddiqi, N.A. (1993). Land from the sea: The mangrove afforestation program of Bangladesh. Ocean and Coastal Management, vol. 20, no. 1, pp. 23-39.

Sasmito, S., Murdiyarso, D., Friess, D., and Kurnianto, S. (2016). Wetlands Ecology and Management

Simard, M., Fatoyinbo, L., Smetanka, C. et al. (2019). Mangrove canopy height globally related to precipitation, temperature and cyclone frequency. Nature Geoscience 12, 40–45

Snedaker, S. C. 1982. Mangrove species zonation: Why?, Tasks for Vegetation Science, Vol. 2., p. 111-125.

Tanino, Y., Nepf, H. M. Laboratory investigation of mean drag in a random array of rigid, emergent cylinders. J. Hydraul. Eng. 134, 34–41. https://doi.org/10.1061/(asce)0733-9429(2008)134:1(34) (2008).

Trampanya, U. (2006). Mangroves and sediment Dynamics along the Coasts of Southern Thailand. Ph.D. Thesis, Wageningen University and Research, Wageningen, The Netherlands.

Uddin, M., Hossain, M.K. (2013). Growth performance of coastal plantations and land stabilization in an offshore Island of Hatiya, Noakhali, Bangladesh. Bangladesh Journal of Forest Science 32.

Van der Meer, J. W., Allsop, N. W. H., Bruce, T., De Rouck, J., Kortenhaus, A., Pullen, T., Schuttrumpf, H., Troch, P. & Zanuttigh, B. 2018. Manual on wave overtopping of sea defences and related structures. An overtopping manual largely based on European resreach, but for worldwide application. www.overtopping-manual.com: EurOtop.

Van Hespen, R., Hu, Z., Peng, Y., Borsje, B.W., Kleinhans, M., Ysebaert, T., Bouma, T.J. (2021). Analysis of coastal storm damage resistance in successional mangrove species. Limnology and Oceanography 66.

Van Rooijen, A. A., McCall, R. T., van Thiel de Vries, J. S. M., van Dongeren, A. R., Reniers, A. J. H. M., Roelvink, J. A. (2016), Modeling the effect of wave-vegetation interaction on wave setup, J. Geophys. Res. Oceans, 121, 4341–4359, doi:10.1002/ 2015JC011392.

Van Wesenbeeck, B.K., Wolters, G., Antolínez, J.A., Kalloe, S.A., Hofland, B., de Boer, W.P, Çete, C., Bouma, T.J. (2021). Wave attenuation through forests under extreme conditions. Scientific Reports.

Van Zelst, V.T.M., Dijkstra, J.T., van Wesenbeeck, B.K. et al. (2021). Cutting the costs of coastal protection by integrating vegetation in flood defences. Nature Communications 12.

Vo Luong, P., Massel, S. (2008). Energy dissipation in non-uniform mangrove forests of arbitrary depth. Journal of Marine Systems. 74. 603-622. 10.1016/j.jmarsys.2008.05.004.

Vuik, V., Jonkman, S.N., Borsje, B.W., Suzuki, T. (2016). Nature-based flood protection: The efficiency of vegetated foreshores for reducing wave loads on coastal dikes. Coastal Engineering 116: 42-56.

Vuik V., van Vuren S., Borsje B.W., van Wesenbeeck B.K., Jonkman S.N. (2018) Assessing safety of nature-based flood defenses: Dealing with extremes and uncertainties. Coastal Engineering 39, Pages 47–64

Vuik V., Borsje B.W., Willemsen P.W.J.M., Jonkman S.N. (2019) Salt marshes for flood risk reduction: Quantifying long-term effectiveness and life-cycle costs. Ocean and Coastal Management 171. Pages 96-110

Wang, G., Zhang, Y., Guan, D., Xiao, L., Singh, M. (2021). The potential of mature Sonneratia apetala plantations to enhance carbon stocks in the Zhanjiang Mangrove National Nature Reserve. Ecological Indicators, 133.

White, F.M., (1991). Viscous Fluid Flow, 2nd ed. McGraw-Hill, New York.

Woodroffe, C., Rogers, K., McKee, K., Lovelock, I., C.E.and Mendelssohn, and Saintilan, N. (2016). Mangrove Sedimentation and Response to Relative Sea-Level Rise. Annual Review of Marine Sciences 8

World Bank (2013). Project Appraisal Document of People's Republic of Bangladesh Coastal Embankment Improvement Project-Phase 1 (CEIP-1) (P128276). Report No.: PAD432

Zhang, Y., Yang, Y., Yang, K., Tan, X., Sun, X., Leng, B., Zhou, C., Zhu, B. (2021). Non-linear wave attenuation quantification model improves the estimation of wave attenuation efficiency of mangroves. Estuarine, Coastal and Shelf Science 245.

Zhu, D., Hui, D., Wang, M. et al. (2021). Allometric growth and carbon storage in the mangrove Sonneratia apetala. Wetlands Ecol Manage 29, 129–141

Appendix A: Mangrove tree geometry

A.1. Methodology for estimating tree area from images

Predicting wave attenuation by mangroves requires describing the frontal tree area, including roots, trunk, and canopy. A literature study (Section 2) provided information about the trunk and roots of mangrove trees, but no information was found for the canopy. The canopy area of *S. apetala* trees is thus obtained by digitizing images collected by Rosanna van Hespen in China. The images are scaled assuming a pneumatophore height of 15 cm, based on personal communication with Rosanna. The contour of the trunk and branches is digitized in Photoshop and read as a binary image in MATLAB. Over the height of the tree, the number of pixels corresponding with the tree area are summed to obtain the vertical distribution of the exposed surface. The total tree area is divided by the tree height to calculate an equivalent tree width b_v, which is normalized using the d_{BH} of the tree (b_v/d_{BH}). For a given tree age, the height and d_{BH} are obtained from a fit to the data of *S. apetala* trees from Bangladesh shown in Figure 2.2. The equivalent tree width is obtained by multiplying the normalized b_v value by the d_{BH}.

A.2. Results of tree area

The images provided by Rosanna van Hespen (Figure A1 and Figure A2) were taken from different perspectives and lighting, which hindered programming algorithms to detect the tree canopy area. Overexposure and shadowing resulted in branches and leaves being partly colored and partly black and white, which made it difficult to define color thresholds for the different tree parts. Moreover, due to low resolution in some images, the smallest branches (with diameters approximately below 1 cm) cannot always be distinguished in the pictures. The analysis thus focuses on the image with the best resolution and color homogeneity (Figure A1), and the results are compared with a second specimen photographed with less quality (Figure A2).

Figure A1. (Left) Photo of S. apetala tree from Rosanna van Hespen. (Center) Digitized root, trunk, and branch area. (Right) Digitized trunk and partial branch area, neglecting small branches with diameters approximately below 1 cm.

For the highest quality picture (Figure A1, left), the total tree area (neglecting leaves) is 1.5 m^2 (Figure A3, left), and it is associated to a diameter at breast height of $d_{BH} = 0.13$ m and a tree height of $h_v = 3.46$ m. The equivalent tree width, obtained by dividing the tree area by the tree height, is equal to 3 times the diameter at breast height ($b_v = 3\ d_{BH}$). The canopy starts at $h_{canopy,min} = 1$ m from the ground, corresponding with 29% of the tree height ($h_{canopy,min} = 0.29\ h_v$), although this value is most likely underpredicted due to the perspective from which the picture was taken. Removing the smallest branches and the pneumatophores (Figure A3, center) reduces the total tree area from $A = 1.5$ m^2 to $A = 0.94$ m^2 and decreases the equivalent tree width from $b_v = 3\ d_{BH}$ to $b_v = 2.1\ d_{BH}$.

A second *S. apetala* specimen where the smallest branches are not distinguisible (Figure A2) is also digitized and results in a diameter at breast height of $d_{BH} = 0.08$ m, a tree height of $h_v = 2.62$ m, a total area of $A = 0.56$ m^2 (Figure A3, right), and an equivalent width of $b_v = 2.6\ d_{BH}$. For the second specimen, the canopy starts at $h_{canopy,min} = 0.32$ m above the ground, corresponding with 12% of the tree height ($h_{canopy,min} = 0.12\ h_v$). The vertical distribution of the tree areas (Figure A3) shows a maximum at the canopy. Despite its simplifications, this analysis suggests that, even neglecting the leaves, a significant fraction of the tree surface is located at the canopy.

Figure A2. (Left) Photo of S. apetala tree from Rosanna van Hespen. (Right) Digitized trunk and partial branch area, neglecting small branches with diameters approximately below 1 cm.

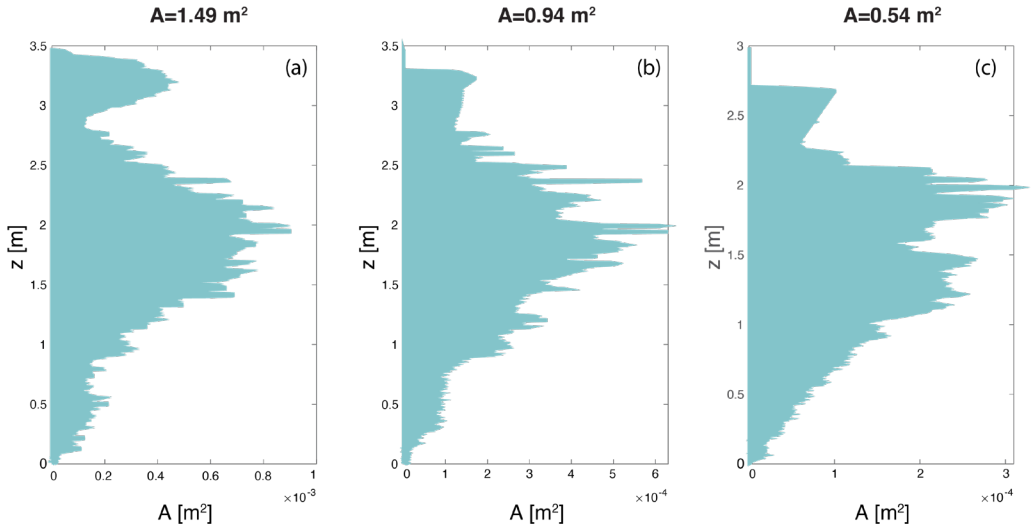

Figure A3. Vertical distribution of the tree area for (a) the S. apetala tree area of Figure A1 (center), (b) the S. apetala tree area of Figure A1 (right), and (c) the S. apetala tree area of Figure A2 (right).

A.3. Modeling of geometrical properties of Sonneratia apetala mangroves

The vertical structure of the mangrove trees is defined by combining information from the literature (Table 2) and from the analysis of field pictures collected by Rosanna van Hespen in China (see Section A.1 and Section A.2). Three tree sections are considered: roots, trunk, and canopy (Figure A4 a). The root height is assumed to correspond with 4% of the

tree height ($h_{root} = 0.04\ h_v$), and the total root width (adding the width of all the pneumatophores), is set equal to 10 times the diameter at breast height ($b_{root} = 10\ d_{BH}$). The canopy is assumed to start at 33% of the tree height ($h_{canopy,min} = 0.33\ h_v$). Considering a total canopy area equal to $A_{canopy} = 2.5\ d_{BH} h_v$ (see Section A.2), a trapezoidal canopy with the same area would have a maximum width of $b_{canopy,max} = 7\ d_{BH}$. The resulting tree structure as a function of the distance from the ground is shown in Figure A4 (b). The evolution of the tree structure as a function of age (using the growth relationships from Figure 2.2) is shown in Figure A4 (c).

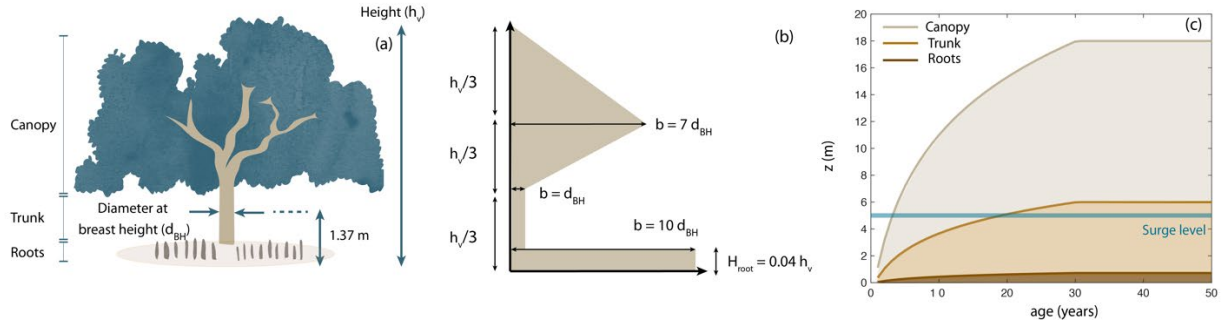

Figure A4. (a) Tree structure. (b) Tree width as a function of the distance from the ground. (c) Height of the different tree sections (canopy, trunk, and roots) as a function of age.

Appendix B: Wave and embankment design model

B1. Wave reduction by mangroves

Predicting the effect of mangroves on coastal embankments requires estimating wave propagation through the forest. Wave attenuation by mangrove trees is directly proportional to the wave loads acting on the vegetation. Wave-driven forces are often represented using the Morison equation (Morison et al., 1950):

$$F_w = \frac{1}{2}\rho c_{D,w} A N_v u^2 + \rho c_M V N_v \frac{du}{dt} \quad (2)$$

where F_w is the force acting on the trees per unit area (N/m^2), which consists of a drag term dependent on the flow velocity squared (left term) and an inertial term dependent on the flow acceleration (right term). ρ is the water density (kg/m^3), $c_{D,w}$ is the (empirical) drag coefficient for waves (-), A is the frontal tree area perpendicular to the wave direction (m^2), N_v is the number of trees per unit m^2, and u is the wave-driven water velocity relative to the tree motion (m/s). If a tree is rigid, the relative velocity will be equal to the velocity of the water particles, and the exposed tree area will remain constant over time. If a tree moves with the waves, its relative velocity and area will change. For trees that do not oscillate but bend to more streamlined shapes, the exposed area reduces under wave loads. In the inertial force component, c_M is an empirical inertia coefficient (-), V is the volume of the tree (m^3), and du/dt is the wave-driven flow acceleration (m/s^2).

The average wave energy dissipated over a wave cycle ϵ_v is equal to the work done by the drag forces, resulting in Equation 3:

$$\epsilon_v = \frac{1}{T}\int_0^{h_v}\int_0^{T}(F_w u)dzdt \quad (3)$$

where h_v is the vegetation height (m) and T is the wave period (s). Mendez and Losada (2004) developed an expression for the wave dissipation ϵ_v assuming negligible plant

motion, that the wave-driven flow can be defined using linear wave theory, and that waves are irregular and follow a Rayleigh distribution, resulting in Equation 4:

$$\epsilon_v = \frac{1}{2\sqrt{\pi}} \rho c_{D,w} b_v N_v \left(\frac{k_p g}{2\sigma_p}\right)^3 \frac{\sinh^3(k_p h_v) + 3\sinh(k_p h_v)}{3k_p \cosh(k_p h)} H_{rms}^3 \quad (4)$$

where b_v is the average plant width (m), k_p is the wave number associated to the peak wave period (rad/m), σ_p is the frequency associated to the peak wave period (rad/s), h is the water depth (m), and H_{rms} is the root mean square wave height (m).

The wave height reduction across a vegetation field can then be calculated by including the expression for ϵ_v (Equation 3 if the vegetation properties vary over the vertical, or Equation 4 for depth-uniform vegetation) in the wave energy balance:

$$\frac{dEc_g}{dx} = -\epsilon_v - \epsilon_b \quad (5)$$

where Ec_g is the wave energy flux, equal to the product of the wave energy E (J/m^2) times the wave group celerity c_g (m/s), and x is the distance in the cross-shore direction (m). According to Equation 5, any wave energy losses across the profile are due to dissipation by the vegetation (ϵ_v) or due to dissipation by wave breaking (ϵ_b), as the effect of bottom friction is assumed negligible in comparison with ϵ_v (Mendez and Losada, 2004).

Energy dissipation due to wave breaking is calculated using the method of Thornton and Guza (1983):

$$\epsilon_b = \frac{3\sqrt{\pi}}{16} \rho g \frac{B^3 f_p}{\gamma_{br}^4 h^5} H_{rms}^7 \quad (6)$$

where f_p is the peak frequency (s^{-1}), and B (-) and γ_{br} (-) are empirical coefficients that are set to the default values used by Mendez and Losada (2004): $B = 1$ and $\gamma_b = 0.6$.

B.2. Embankment height design

The height of an embankment is usually chosen in such a way that the overtopping discharge remains below a critical threshold, which depends on the erosion resistance of the crest and inner slope of the embankment. Mangroves reduce the value of H_{m0} at the structure, and thus decrease the overtopping discharge for a given design. The overtopping discharge over a structure q can be calculated using empirical equations, such as the equation of van der Meer (2018):

$$q = \sqrt{g \cdot H_{m0}^3} \cdot \frac{0.026}{\sqrt{\tan \alpha}} \cdot \gamma_b \cdot \xi_{m-1,0} \cdot e^{-\left(2.5 \frac{h_{crest}-h}{\xi_{m-1,0} \cdot H_{m0} \cdot \gamma_b \cdot \gamma_f \cdot \gamma_\beta \cdot \gamma_v}\right)^{1.3}}, \quad (7)$$

where q is the overtopping discharge per meter (m^2/s), g is the gravitational acceleration (m/s^2), and H_{m0} is the spectral significant wave height (m), which relates to H_{rms} according to $H_{m0} = \sqrt{2} H_{rms}$. α is the angle of the outer slope (-), $\xi_{m-1.0}$ is the breaker parameter (-), γ_b is the influence factor for a berm (-), γ_f is the influence factor for roughness elements on the slope (-), γ_β is the influence factor for oblique wave attack (-), γ_v is the influence factor for vertical wall, h_{crest} is the crest level (m), and h is the water level (m).

B.3. Slope protection design

Wave attenuation by mangroves can also reduce the stone weight required to protect the embankment slope. The slope protection of the embankment can be calculated with the expression of Pilarczyk (1990,1998).

$$\frac{H_{m0}}{\Delta D} = \frac{F \cos \alpha}{\xi_{m-1.0}^b} \quad (8)$$

where H_{m0} is the spectral significant wave height at the toe of the structure (m), D is the thickness of the cover layer (m), Δ is the relative density of concrete with respect to water (-), F

is a stability factor equal to 3.5 for a revetment formed by concrete blocks (-), and b is an exponent equal to 0.66 for semi-permeable block revetments.

B.4. Erosion at the toe

Wave attenuation by mangroves reduces the shear stresses acting at the toe of the embankment, and hence decreases the erosion rates. The effect of wave attenuation by mangroves on the shear stresses (τ_w) acting on the embankment toe can be calculated according to Equation 9:

$$\tau_w = \frac{1}{4}\rho f_w u_{rms}^2 \tag{9}$$

where f_w is an empirical friction factor (-) and u_{rms} is the near-bed velocity associated to H_{rms} (which decreases in the presence of a mangrove belt) in m/s. The friction factor can be determined as:

$$f_w = \min\left(\exp\left(-6 + 5.2\left(\frac{u_{rms}}{2.5 D_{n50}\omega_m}\right)^{-0.19}\right), 0.3\right) \tag{10}$$

with D_{n50} being the mean grain size (m) and ω_m the mean wave frequency (rad/s).

B.5. Wind loads

Wind loads on trees are often parameterized using a quadratic drag law:

$$F_a = \frac{1}{2}\rho_a c_{D,c} A G u_a^2 \tag{11}$$

where ρ_a is the air density (kg/m^3), $c_{D,c}$ is the drag coefficient for wind currents (-), A is the frontal tree area (m^2), G is an empirical gust factor (-), and u_a is the wind speed relative to the tree motion (m/s). Above the vegetation, the wind speed is often assumed to follow a logarithmic velocity profile over the vertical coordinate z (Gardiner et al., 2016):

$$u_a(z) = \frac{u_a^*}{k} \ln\left(\frac{z}{z_0}\right) \tag{12}$$

where z_0 is the roughness height (m), which can reach values of the order of 0.02 m for unvegetated sites and 5 m for forest areas, u_a^* is the friction velocity (m/s), and k is the von Karman constant (-), equal to 0.4. Between the trees, the wind velocity is often assumed to follow an exponential decay towards the ground (Kaimal et al., 1994):

$$\frac{u_a(z)}{u_a(h_v)} = e^{-\upsilon_e(1-z/h_v)} \tag{13}$$

with υ_e being an empirical reduction factor (-), and h_v being the tree height. The empirical gust factor G is given by Equation 14 (Gardiner et al., 1997):

$$G = \frac{\left(2.7193\left(\frac{D}{h_v}\right) - 0.061\right) + \left(-1.273\left(\frac{D}{h_v}\right) + 0.9701\right)\left(1.1127\left(\frac{D}{h_v}\right) + 0.0311\right)^{x/h_v}}{\left(0.68\left(\frac{D}{h_v}\right) - 0.0385\right) + \left(-0.68\left(\frac{D}{h_v}\right) + 0.4785\right)\left(1.7239\left(\frac{D}{h_v}\right) + 0.0316\right)^{x/h_v}} \tag{14}$$

where D is the average separation between trees (m), h_v is the tree height, and x is the distance from the edge of the forest (m).

B.6. Tree resistance

Trunk breakage (Figure 2.4, b) can be estimated by comparing the bending moment caused by the forces acting on the tree (Equation 2 for waves, and Equation 11 for wind) with the maximum bending moment that a tree can withstand without breaking, M_{break} (Quine and Gardiner, 2007):

$$M_{break} = \frac{\pi}{32} f_{knot} \sigma_u \, d_{BH}^3 \tag{15}$$

where σ_u is the modulus of rupture of the wood tissue (N/m^2), d_{BH} is the trunk diameter at breast height (m), and f_{knot} is a factor that reduces the wood strength due to the presence of knots (-), usually between f_{knot} = 0.8-1. Van Hespen et al. (2021) measured σ_u values 37±7 N/mm^2 for *S. apetala* branches.

Overturning, which is often modeled combining mechanisms (a) and (d) of Figure 2.4, can also be estimated by comparing the bending moment acting on the tree with the critical overturning moment M_{over}, measured in tree pulling experiments (Nicoll et al., 2006):

$$M_{over} = C_r W \tag{16}$$

where C_r is a dimensional regression constant varying between C_r = 60-200 m^2/s^2, and W is the tree trunk weight in kg.

B.7. Modeling mangrove failure against wind and wave loads

At every grid point the bending moment is calculated and compared with the maximum threshold for trunk breakage and tree overturning. The bending moment acting on the tree is calculated for wind loads using Equation 11 and for wave loads using Equation 2, by multiplying the total force of each segment times its distance to the ground. Vegetation motion is neglected for both wave and wind loads.

For wind loads, we assume that the input wind speed is measured 10 m above the ground at a location without vegetation (Figure B1). Since the velocity profile changes between sites with and without vegetation, we calculate the corresponding velocity 200 m from the ground using Equation 12 with $z_0 = 0.02$ (Gardiner et al., 2016). We assume the wind has the same speed at 200 m from the ground for vegetated and unvegetated areas, and that the wind velocity differs between both sites below this elevation. The velocity on top of the forest is calculated using Equation 12, assuming a rough boundary layer with a roughness height of $z_0 = h_v/30$, where h_v is the tree height. The velocity between the trees is then calculated using an exponential velocity decay (Equation 13) with a reduction factor of $\upsilon_e = 1$. This decay is applied inside the forest, but not at the seaward edge.

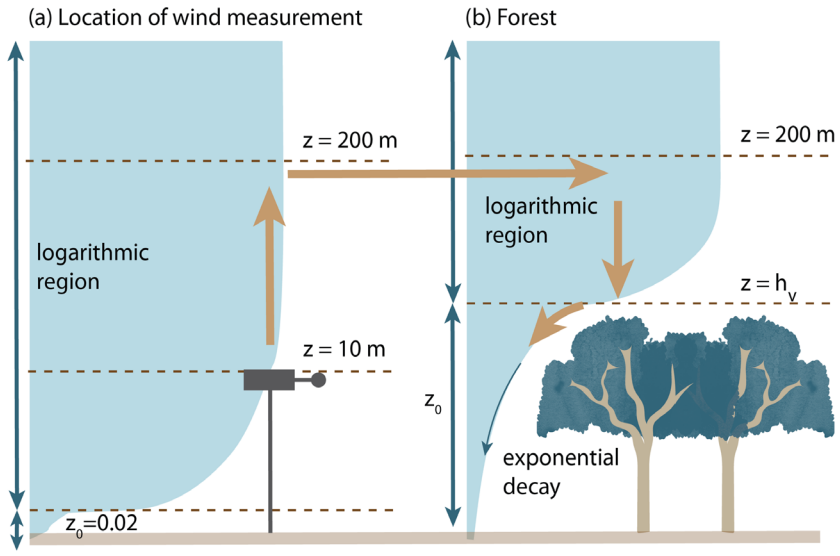

Figure B1. Assumptions for wind velocity profiles. (a) Input wind velocities are assumed to correspond with a wind station at an unvegetated area, where the velocities are measured 10 m above the ground. The corresponding velocity 200 m from the ground is calculated assuming a logarithmic boundary layer. The velocity 200 m above the forest is assumed equal to the value of the unvegetated site. Inside the canopy, an exponential velocity decay is applied.

The resisting moment against breakage (Equation 15) is derived using the σ_u values from van Hespen et al. (2021) and assuming $f_{knot} = 1$. For tree overturning (Equation 16), the full range of C_r values from the literature is considered. The tree weight, used as an input in Equation 16, is computed using the allometric relationships from Zhu et al. (2021).

Appendix C: Validation of the wave model

The wave transformation model is validated against field wave measurements collected at a salt marsh fringe by Vuik et al. (2016). Wave propagation through the salt marshes is modeled for a significant wave height of $H_{m0} = 0.6$ m and a peak period of $T_p = 3.5$ s at the offshore boundary. The bathymetry varies between an offshore water depth of 2 m, and a nearshore water depth of 0.5 m. The salt marshes extend over a length of 55 m and have varying vegetation properties across the profile, but uniform properties over the vertical coordinate. The vegetation properties are summarized in Table C1. A drag coefficient of $c_{D,w} = 0.4$ is used in the simulations, which is equal to the value calibrated by Vuik et al. (2016).

Table C1. Salt marsh properties used for the validation from Vuik et al. (2016), consisting of the mean vegetation height h_v, the mean stem density N_v, and the mean stem width b_v. The location of the sections across the profile is indicated in Vuik et al. (2016).

Section	$h_{v,\,mean}$ (m)	N_v (plants/m^2)	b_v (m)
S1-S2	0,2	944	0,030
S2-S3	0,29	1136	0,034
S3-S4	0,27	1520	0,037

The wave propagation model shows good agreement with the model predictions and field measurements of Vuik et al. (2016), as shown in Figure C1. The agreement is good both for a situation without vegetation, and with vegetation, which indicates that both wave breaking and the vegetation module are well implemented.

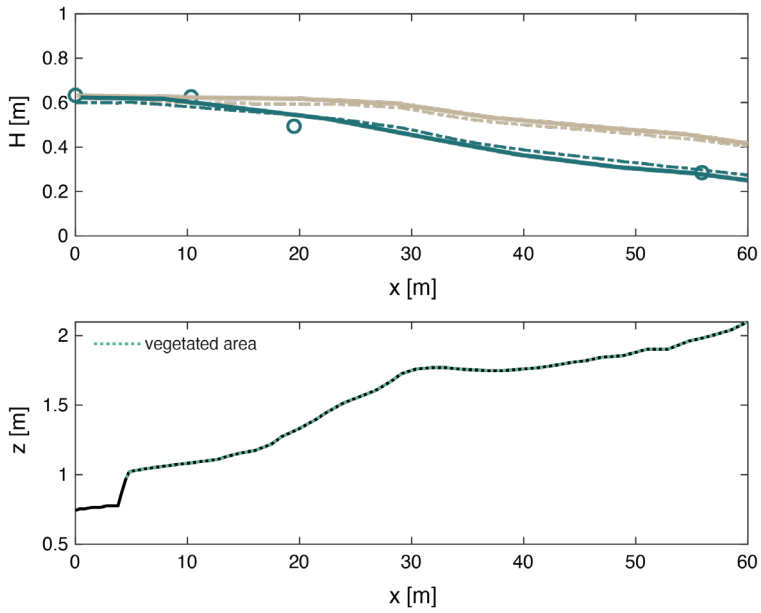

Figure C1. (Top) Comparison between the model presented in Appendix B and the SWAN model and field measurements by Vuik et al. (2016). The results obtained with an unvegetated profile are shown in brown, and the results obtained with a vegetated profile in green. The model results of this study are presented in a dashed line, and the results of Vuik et al. (2016) in solid lines. Measurements are shown by green dots. (Bottom) Bathymetry used in the simulations. The vegetated region is shown in green.

The wave model is also validated against measurements of wave propagation through willow trees, collected in large-scale flume experiments (van Wesenbeeck et al., 2022). The experimental set-up consisted of 32 willow trees that were installed in a concrete platform, over a length of 40 m (Figure C2, a). Waves were generated at one side of the flume, propagated through the vegetation, and reached a dike at the opposite side of the flume. The wave heights were recorded just upstream from and downstream of the trees. The tested waves varied between offshore significant wave heights of $H_{m0} = 0.43 - 1.44$ m, associated to peak wave periods ranging between $T_p = 2.84 - 6.65$ s. The water depth was varied between $h = 3 - 4.5$ m in the experiments. The surface area of the trees as a function of height is obtained from Kalloe et al. (2022) (shown in Figure C2, b), and the input drag coefficients were obtained from van Wesenbeeck et al. (2022).

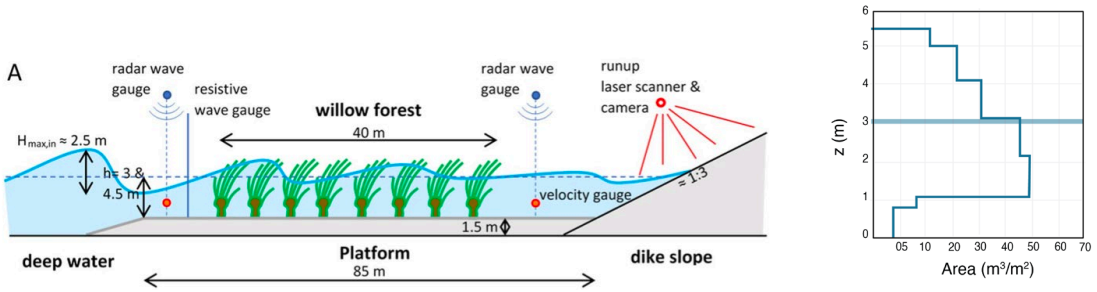

Figure C2. (a) Set up of the flume experiments done by Wesenbeeck et al. (2022) with large-scale willow trees. (b) Measured tree area over the vertical coordinate.

The vegetation module also shows good agreement with laboratory measurements by van Wesenbeeck et al. (2022) (Figure C3), which were collected for trees with vertically varying geometry (Figure C2).

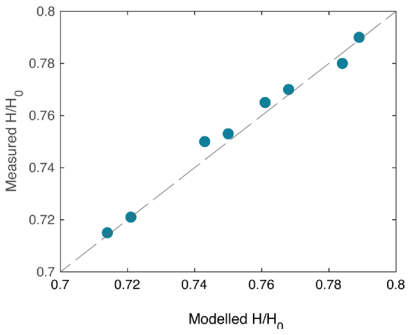

Experiment	h [m]	Hrms [m]	Tp [m]	Cd_canopy	H/H0 meas	H/H0 model
1	3	0,304	2,84	2,24	0,715	0,714
2	3	0,685	3,92	1,19	0,726	0,721
3	3	0,332	3,93	1,87	0,780	0,784
4	3	0,671	5,57	1,17	0,753	0,750
5	3	0,311	2,84	1,64	0,770	0,768
6	3	0,671	3,57	1,02	0,750	0,743
7	3	0,318	3,93	1,84	0,790	0,789
8	3	0,685	5,57	1,07	0,765	0,761

Figure C3. (Left) Comparison between model predictions of wave propagation through a willow forest against laboratory measurements of van Wesenbeeck et al. (2022), where H is the wave height transmitted through the forest and H_0 is the incoming wave height at the edge of the forest. (Right) Table summarizing the water level (m), incoming wave height (m), wave period (s), canopy drag coefficient (-), measured wave transmission through the forest (-), and the wave transmission calculated using the model of Appendix B (-).

Appendix D: Drag coefficient for mangroves in Bangladesh

Wave attenuation largely depends on the value of the drag coefficient. The drag coefficient of *S. apetala* branches was estimated in a set of flume experiments by van Hespen et al. (2021). In their tests, tree branches were exposed to waves and currents, and forces and flow velocities were measured to fit $c_{D,w}$. Drag coefficient measurements from experiments with waves vary between $c_{D,w} = 2 - 6$, and from experiments with a combination of waves and currents between $c_{D,w} = 2.8 - 4.3$. These values exceed the drag coefficient for rigid single cylinders, which tend to $c_{D,c} = 1$ in currents (White, 1991), $c_{D,w} = 1 - 2.5$ in waves (Keulegan and Carpenter, 1958). Van Hespen et al. (2021) reported that their measurements probably overpredict the drag coefficients expected in the field, as in reality the branches of a tree may shelter each other from the flow. Their drag values could also be larger than for rigid isolated cylinders due to flow acceleration effects between the branches (Tanino and Nepf, 2008; Etminan et al., 2019), but also due to scaling effects. The latter is a likely contributing factor as large-scale flume experiments with real-scale willow trees provided drag coefficients between $c_{D,w} = 0.5 - 2.5$ (van Wesenbeeck et al., 2022), where the largest $c_{D,w}$ values showed good agreement with Keulegan and Carpenter (1958). The smallest $c_{D,w}$ values for willows were obtained for the highest KC values, where KC represents the ratio of wave excursion to branch diameter. Those wave conditions were associated with the largest tree motion, which resulted in smaller $c_{D,w}$, values compared to rigid elements. Drag reduction due to plant motion will most likely play a role for young mangrove specimens, with thinner and more flexible branches compared to mature trees.

Appendix E: Sensitivity analysis

E.1. Sensitivity of wave energy dissipation by mangrove trees to the vegetation properties

The effect of changing all tree properties ($d_{BH}, h_v, c_{D,w}, N_v$) within +/- 30% on wave dissipation is shown in Figure E1. For these scenarios, we consider combination of parameters where all values are kept the same as in a reference situation, except for one parameter that is either increased or decreased by 30%. The accumulation of uncertainties in vegetation growth and hydrodynamics has a significant effect on wave dissipation, with the maximum possible dissipation being 10 times larger than the smallest value.

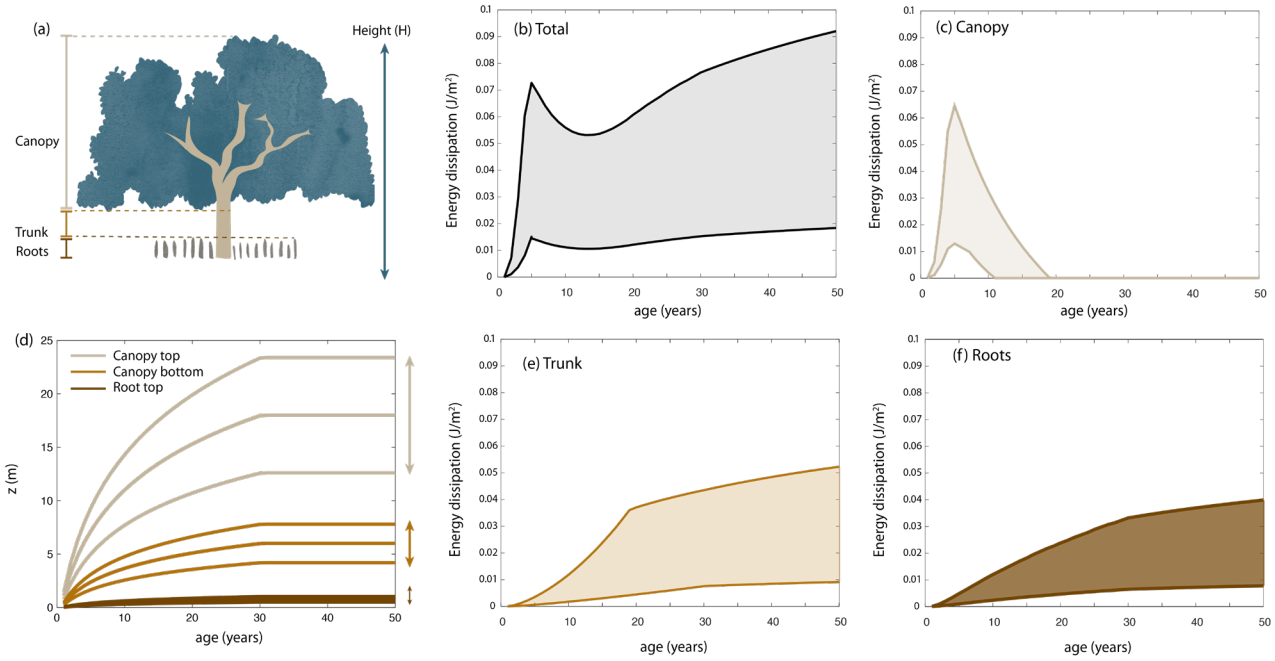

Figure E1. (a) Tree structure, and variability in the height of the different parts of the tree (d). Wave dissipation by (b) the full tree, (c) the canopy, (e) the trunk, and (f) the roots.

E.2. Effect of surge height on wave attenuation

The effect of the surge levels on wave attenuation by a 100 m belt is evaluated for different forest ages in Figure E2 for $c_{D,w} = 0.7$ (Figure E2, b) and for $c_{D,w} = 1.3$ (Figure

E2, c). Wave attenuation is minimum for intermediate surge levels between 2.5-5 m. For water levels below 2.5 m, the dense roots of the trees cover a significant part of the water column and increase wave dissipation by the trees. For water levels above 5 m, larger waves can reach the vegetation without breaking, which increases wave dissipation by the mangroves. The wave attenuation predictions are also quite dependent on the vegetation resistance. For instance, increasing the drag coefficient from $c_{D,w} = 0.7$ to $c_{D,w} = 1.3$ increases the wave height reduction by a 50-year-old mangrove belt from 6% (Figure E2, b) to 10% (Figure E2, c) for a wave height of 2 m and a surge level of 5 m.

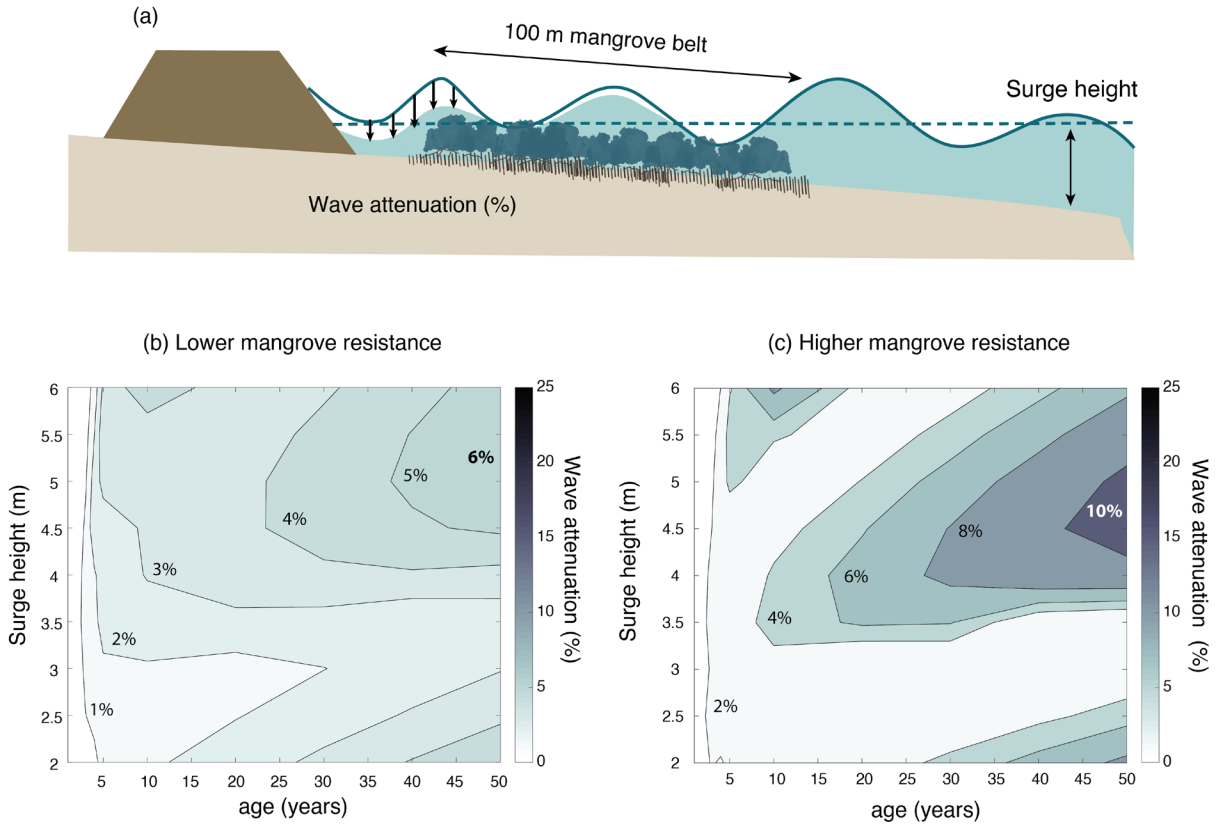

Figure E2. (a) Effect of surge level on wave attenuation by a 100 m mangrove belt with respect to a situation without mangroves. Plots (b) corresponds with the geometrical tree model presented in Figure A4, $c_{D,w} = 0.7$ and $N_v = 0.1$ trees/m^2. Plots (c) corresponds with the same tree model and modeling parameters except for a larger drag coefficient of $c_{D,w} = 1.3$.

E.3. Effect of the slope on wave attenuation

The profile slope influences the potential effect of a mangrove belt by (1) limiting its maximum extension and, (2) by changing the water depth, and thus the wave attenuation

rates, through the trees. Considering that mangroves grow between MSL and MHW, and assuming a tidal range of approximately 2 m, slopes of 1/10, 1/100 and 1/1000 result in maximum mangrove forest lengths of 10, 100 and 1000 m respectively. If the water level at the landward end of the forest is set to a fixed value, a steeper slope increases the water depth through the vegetation. When a mangrove belt with a width of 10 m is modeled with slopes of 1/10, 1/100 and 1/1000, wave attenuation by the forest remains below 3% for all cases (Figure E3). For a wider belt of 100 m, reducing the slope from 1/100 to 1/1000 increases wave attenuation from 4-10% to 5-14% for a 50-year-old forest (Figure E4).

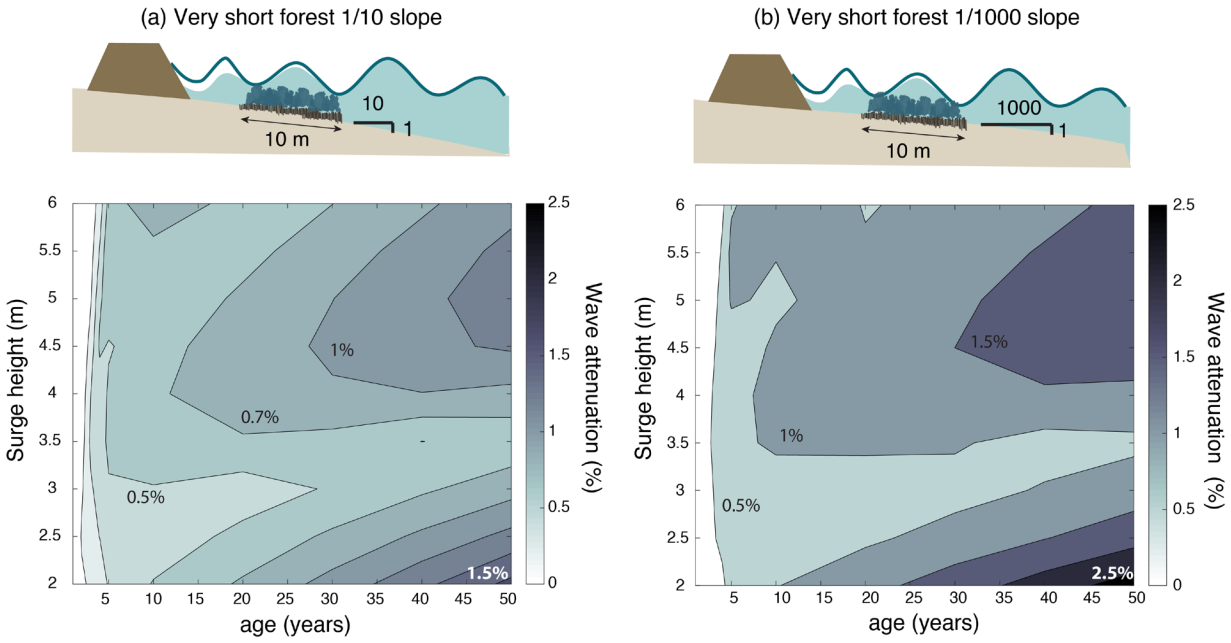

Figure E3. Wave attenuation through a 10 m wide mangrove forest. Plot (b) corresponds with the geometrical tree model presented in Figure A4, $c_{D,w} = 1.3$, $N_v = 0.1$ trees/m^2, and a slope of 1/10. Plot (c) corresponds with the geometrical tree model and modeling parameters, except for a milder slope of 1/1000.

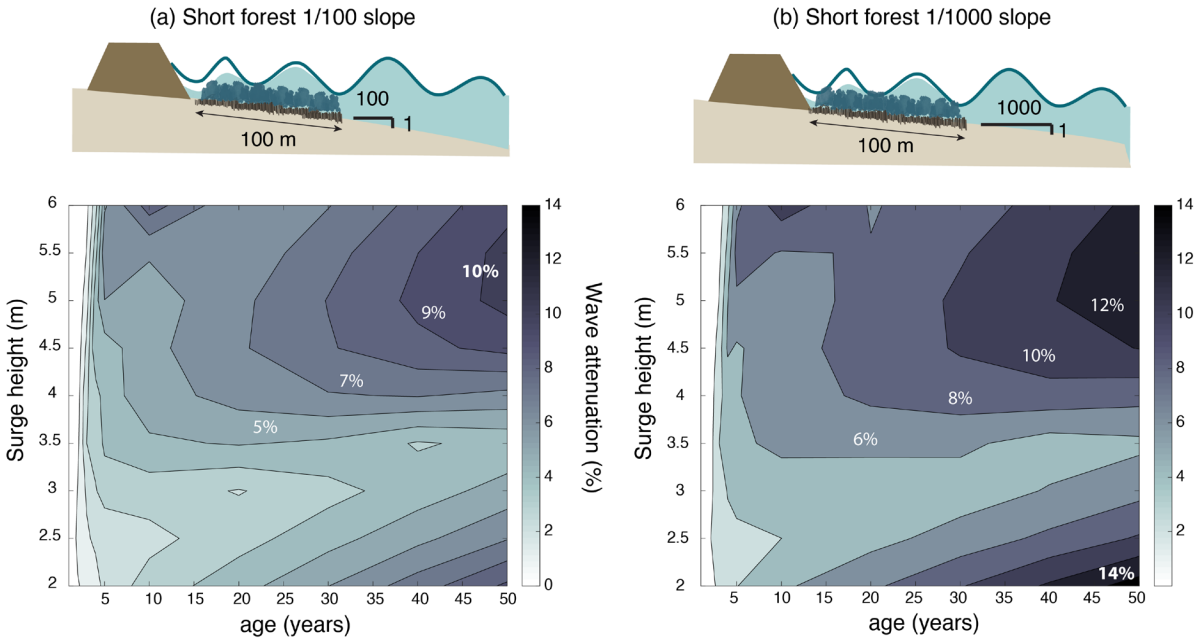

Figure E4. Wave attenuation through a 100 m wide mangrove forest. Plot (b) corresponds with the geometrical tree model presented in Figure A4, $c_{D,w} = 1.3$, $N_v = 0.1$ trees/m^2, and a slope of 1/100. Plot (b) corresponds with the same geometrical and modeling parameters except for a milder slope of 1/1000.